Copyright Undertaking

This thesis is protected by copyright, with all rights reserved.

By reading and using the thesis, the reader understands and agrees to the following terms:

1. The reader will abide by the rules and legal ordinances governing copyright regarding the use of the thesis.

2. The reader will use the thesis for the purpose of research or private study only and not for distribution or further reproduction or any other purpose.

3. The reader agrees to indemnify and hold the University harmless from and against any loss, damage, cost, liability or expenses arising from copyright infringement or unauthorized usage.

THE HONG KONG POLYTECHNIC UNIVERSITY

DEPARTMENT OF INDUSTRIAL AND SYSTEMS ENGINEERING

Microwave Sintering of Polypropylene / Carbon Nanotube / Hydroxyapatite Composites

CHEN XU

A thesis submitted in partial fulfilment of the requirements for the degree of Master of Philosophy

June 2011

CERTIFICATE OF ORIGINALITY

I hereby declare that this thesis is my own work and that, to the best of my knowledge and belief, it reproduces no material previously published or written, nor material that has been accepted for the award of any other degree or diploma, except where due acknowledgement has been made in the text.

_____ (Signed)

_____CHEN XU_____ (Name of student)

ABSTRACT

Abstract of thesis entitled "Microwave sintering of polypropylene / carbon nanotube / hydroxyapatite composites"

Submitted by <u>CHEN XU</u>

For the Degree of Master of Philosophy

at the Hong Kong Polytechnic University in June, 2011

The microwave sintering technique was developed for the fabrication of microwave transparent polypropylene (PP) based hydroxyapatite (HA) composites as an alternative to conventional polymeric material processing. Several studies were conducted on the microwave sintering of PP composites due to their microwave transparency and low dielectric properties. It was hypothesized that the incorporation of microwave susceptors into the polymer matrix would allow the polymer matrix to be sintered by microwave absorption. In this study, carbon nanotubes (CNTs) and HA particles were used as the microwave susceptors and the bioactive fillers, respectively.

The objectives of the study were to perform microwave sintering of polypropylene/carbon nanotube/hydroxyapatite (PP/CNT/HA) composites, to examine the structure and to investigate the mechanical properties of the resultant composites. The microwave sintering of PP/CNT/HA composites was made feasible by the incorporation of 1 wt% CNT. Moreover, PP/CNT/HA composites with 0, 5, 15 and 30 wt% HA filling were fabricated successfully. In some cases, rapid microwave sintering,

i.e. with a sintering time of less than a minute, was achieved. It was also found that the sintering time decreases with increase of the HA content. The existence of the PP and HA compositions in the microwave sintered composites was confirmed by X-ray diffraction experiments. Homogeneous distribution of HA within the polymer matrix was confirmed by scanning electron microscopy. In order to evaluate the elastic modulus of the fabricated samples, a novel finite element based small punch testing method was developed, which was shown to be more sensitive and accurate than the small punch bending technique that is typically used for small samples. The elastic modulus of the PP/CNT/HA composite was determined as 1.4 ± 0.1 GPa.

To conclude, incorporation of microwave susceptors allows microwave transparent polymer powders to absorb heat and to be subsequently sintered, forming a pre-defined shape. By applying the proposed dispersion method and the microwave sintering technique, PP/CNT/HA composites were prepared successfully.

Acknowledgements

I would like to express my sincere appreciation to my research supervisor Prof. C.Y. Tang for his continuous support throughout this research study. I am forever grateful for what he has sacrificed for my continuing improvement.

My gratitude is also accorded to Miss L. Chen, Dr. C.T. Wong, Dr. C.P. Tsui, Dr. D.Z. Chen and Dr. G. Zhang, for their selfless help, valuable suggestions during the experimentation and simulation in this study.

Finally, I would like to thank my family members and friends for their unyielding support.

Table of Contents

Chapter 1: Introduction

1.1 Background

Microwave processing of materials has attracted great research interest, especially for metals and ceramics (Bykov *et al.*, 2001; Oghbaei *et al.*, 2010; Thostenson *et al.*, 1999). Microwaves are part of the electromagnetic spectrum, with a range between 300 MHz to 300 GHz in frequency and between 1 mm and 1 m in wavelength (Oghbaei *et al.*, 2010). The primary advantage of microwave processing is direct coupling with materials, thus reducing processing time and energy (Bykov *et al.*, 2001; Oghbaei *et al.*, 2010; Thostenson *et al.*, 1999). For microwave composite fabrication, a high bonding strength may be generated between the filler and the matrix, with different dielectric constants due to the soldering effect by microwave selective heating (Wang *et al.*, 2007).

Polypropylene (PP), with high chemical resistance, high dimensional stability and low density, is a polymer having commercial importance in a great number of industrial applications, such as in construction, for automotive components and in fibre manufacturing (Kissel *et al.*, 1999). In order to expand the applications of PP, carbon nanotubes (CNTs) were incorporated into the polymer to improve the mechanical (Kearns *et al.*, 2002), thermal (Valentini *et al.*, 2003), electrical (Seo *et al.*, 2004), as well as biological (Harrison *et al.*, 2007) properties. Due to its mechanical and biological properties, attention has also been paid in the study of PP/HA composites as a biomaterial, analogous to bone, particularly for higher load bearing applications (Liu *et al.*, 2007).

Recently, a number of techniques have been applied for fabricating PP based composites, such as melt blending, extrusion and compression moulding (Esawi *et al.*, 2010; Logakis *et al.*, 2010; Pujari *et al.*, 2009). These techniques involve a conventional heating process, i.e., heat conduction and convection, which may not be the preferred method as compared with microwave processing in terms of energy and time saving.

For polymeric materials, the microwave has been used for curing (Thostenson *et al.*, 1999), welding and joining (Potente *et al.*, 2002), microwave-assisted synthesis (Wiesbrock *et al.*, 2004), and rubber vulcanization (Krieger, 1992). Studies were conducted to investigate the polymer composite responses to a microwave field (Brosseau *et al.*, 2001; Kim *et al.*, 2009; Wu *et al.*, 2004).

The main technical barrier is that most thermoplastic polymers are either transparent to microwaves or have low dielectric loss constants (Meredith, 1998), which means no or little coupling between the materials and microwaves. To overcome this deficiency, external susceptors were used (Cheng *et al.*, 1997; Goldstein *et al.*, 1999) to assist in the processing of the polymeric materials. Actually, the microwave sintering technique for ceramics and metals can be categorized into direct sintering and hybrid sintering, depending on whether the susceptors are incorporated into the sintering materials. CNTs seem to be promising candidate in serving as susceptors, due to their high dielectric loss constants (Wadhawan *et al.*, 2003). Bio-ceramics, such as hydroxyapatite (HA), have been adopted to increase the bioactivity of the implant materials (Liu *et al.*, 2007). The bioactivity often depends on the amount of bioactive materials filling.

In this research, microwave technology was used to fabricate the PP/CNT/HA composites. The microwave sintering technique was developed for the fabrication of microwave transparent PP based composites. The microstructure and the mechanical performance of the resultant composites were also studied.

1.2 Significance and Objectives

The objective of this project is to study the feasibility of processing PP based composites by microwave sintering technique. Microwave processing is among the techniques having great potential to reduce the processing time and the energy consumed. For polymeric materials, this potential has not been fully explored so far. The main technical barrier is that most polymers are either microwave transparent or have low dielectric loss constants. Here, a microwave transparent PP was used as the composite matrix for the microwave processing, and CNTs were introduced as susceptors. Moreover, the effect of HA incorporation on the mechanical properties of the composites was also investigated. A three phase composite system, PP/CNT/HA, was to be developed by microwave processing.

The study is divided into the following tasks:

- To develop a microwave sintering technique to fabricate PP based composites, for which a reduction in processing time is expected to be achieved;

- To characterize the fabricated composites, so as to validate the feasibility of microwave sintering in terms of investigating the dispersion method and sintering condition;

- To develop a technique to evaluate the elastic modulus, particularly for the small specimens fabricated, which may pave the way towards further development in mechanical evaluation for samples that are smaller than standard sizes.

The achievement of the project objective will provide an efficient alternative to process microwave transparent polymers and their composites.

1.3 Organization of the Thesis

There are five chapters in this thesis. Chapter 1 highlights the background, and points out the significance and objectives of this study. Chapter 2 presents a literature review, involving microwave sintering, PP, CNT and HA related composites, as well as current technology barriers. Chapter 3 introduces the experimental process for the fabrication of composites, and presents a series of subsequent characterization test results. A small punch testing technique based on finite element analysis was developed and validated for evaluating the elastic modulus of fabricated samples, and is presented in Chapter 4. Finally, in Chapter 5, overall conclusions together with suggestions for further study are summarized.

Chapter 2: Literature Review

2.1 Microwave Sintering of Materials

In this section, the basics of microwave technology, microwave sintering of polymeric materials, and a comparison between microwave and conventional processing are reviewed.

2.1.1 Microwave Basics

Microwaves are categorized as an electromagnetic spectra with a frequency range of 300 MHz to 300 GHz, and 1 mm to 1 m in wavelength (Oghbaei *et al.*, 2010). Generally, there are two major applications of microwave technology. The first one is in communications such as television, radar and satellite applications, and the second one is in microwave heating. The frequently adopted frequencies for microwave heating are 915 MHz and 2.45 GHz, while microwave furnaces with variable frequencies have also been developed for microwave heating (Meredith, 1998).

As part of the electromagnetic spectrum, an electric field and a magnetic field are two fundamental components for a propagating microwave. Maxwell expressed the interaction between the magnetic and electric fields in his famous Maxwell's Equations, in which the variation of electromagnetic fields with time are described physically (Meredith, 1998). Based on electromagnetic theory, especially using Maxwell's Equations, a microwave furnace can be typically designed with three components:

microwave source, transmission tube and applicator (Thostenson *et al.*, 1999).

The microwave source is a vacuum tube, two typical types of which are the magnetron and the travelling wave tube (TWT). The magnetron has been often adopted in domestic microwave ovens, and was reported to be of a certain reliability and efficiency (Kitagawa *et al.*, 1986). The magnetron not only acts as a creator of oscillation frequency but also acts as a signal amplifier. However, the second type of vacuum tube TWT can only be used to amplify the signal (Lauf *et al.*, 1993).

The transmission tube is actually an energy coupler from the microwave source to the applicator. A waveguide usually serves as the transmission tube, especially at high power and frequencies where the coaxial cables often cause great losses. The waveguide is usually a rectangular hollow tube in which the electromagnetic wave propagates. In the rectangular waveguide, the electromagnetic wave can be depicted as a linear combination of the transverse magnetic (TM) mode and the transverse electric (TE) mode (Thostenson *et al.*, 1999).

A microwave applicator is where the microwave energy is absorbed by the materials. The applicator is a closed chamber with metal walls, which is actually an electromagnetic resonator. For the resonator, there are several eigenmodes, each of which has its resonator frequency, ω_n, and corresponding quality factor Q_n for characterizing excitation frequency. It was suggested that the relationship between the ratio ω_n/Q_n and the frequency difference of the adjacent modes $\Delta\omega$, provides the basis for dividing applicators into multi and single modes. Figure 2.1 below demonstrates the

efficiency difference of the cavity excitation characteristics for single-mode and multi-mode applicators (Bykov *et al.*, 2001).
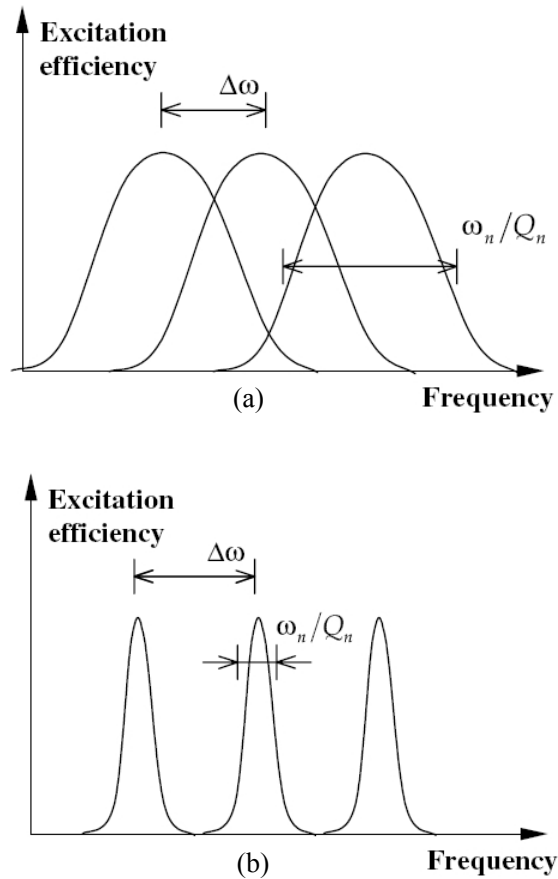
Fig. 2.1 Illustrated curves of the cavity excitation regimes: (a) multi-mode and (b) single-mode (Bykov *et al.* 2001)

The ratio ω_n/Q_n somewhat determines the excitation efficiency. In order to excite an efficient eigenmode, the source frequency of the microwave should satisfy the relationship $|\omega - \omega_n| < \omega_n/Q_n$. When $\omega_n/Q_n > \Delta\omega$, the applicator is multi mode. The

multi-mode applicator allows for a number of modes with high orders at the same time, as observed in the domestic microwave oven. The distribution of microwaves in the multi-mode oven depends on many factors, for example the number of resonance modes probably increases with the size of the microwave cavity. In this manner, the design of the multi-mode applicator is largely based on experience, or a trial-and-error approach (Thostenson *et al.*, 1999). When $\omega_n/Q_n < \Delta\omega$, only one single resonator eigenmode is excited, i.e., single mode. The single mode applicator generates a non-uniform distribution of the magnetic field. Generally, a single mode applicator has a "hot spot", within which the microwave intensity is high (Palaith *et al.*, 1989).

2.1.2 Microwave-Material Interaction Mechanism

Generally, two mechanisms can be used to explain the heating effects of dielectric materials in a microwave field. The first one is that the dielectric materials may act as poor electric conductors, within which heat can be generated because of the finite electrical resistivity. The second one is caused by the heat generated by the friction forces in dielectric materials, as the molecular dipolar components tend to align with the high-frequently-alternated microwave field. A great number of dielectric materials display polar properties. When the frequency rises beyond 100 MHz, the dipolar heating mechanism predominates as compared with conduction effects (Meredith, 1998).

For a dielectric material, the dielectric constant (ε') and the dielectric loss factor (ε'') can somewhat determine the dielectric response in terms of the capacitive and

conductive characteristics. By combining the two components, the complex dielectric constant (ε^*) can be expressed as below in Equation (2-1) (Thostenson *et al.*, 1999):

$$\varepsilon^* = \varepsilon' - i\varepsilon'' \tag{2-1}$$

The dielectric properties of the materials result in a heating effect in the form of electromagnetic energy conversion, under the applied electromagnetic field. A dielectric heating equation, based on the familiar parallel-plate capacitor was reported, as shown in Equation (2-2).

$$p = 2\pi f \varepsilon'' E_i^2 \tag{2-2}$$

where p (W m^{-3}) is the power dissipation density; f (Hz) is the microwave frequency; ε'' is the loss factor of the dielectric material; and E_i is the electric field stress within the dielectric material. According to Equation (2-2), the power dissipation density p is proportional to the loss factor ε'', when the other parameters are constant. It is not claimed to be rigorous but has a clear and simple argument (Meredith, 1998).

The penetration depth of the electromagnetic wave into a dielectric heating workload is another important parameter, as it gives an indication of the heat distribution within the workload. The penetration depth D_p (m) is defined as a depth in the material at which power flux has decreased to $1/e$ (0.368) of the value on the surface. The penetration depth D_p (m) is a function of dielectric constant ε' and loss factor ε'', which is expressed in Equation (2-3) (Metaxas *et al.*, 1983).

$$D_p = \frac{\lambda_0}{2\pi\sqrt{(2\varepsilon'/\varepsilon_0)}} \frac{1}{\sqrt{\left[1+\left(\frac{\varepsilon''}{\varepsilon'}\right)^2\right]^{0.5}-1}} \qquad (2\text{-}3)$$

where λ_0 is the wave length of the electromagnetic wave, ε_0 (F m^{-1}) is the vacuum permittivity, and $\varepsilon'' \leq \varepsilon'$. It is noted that the penetration depth D_p decreases with the frequency of the electromagnetic wave, and with the dielectric constant ε''. For a microwave transparent PP, where both ε' and ε'' can be regarded as zero, the penetration depth D_p could therefore be infinite.

2.1.3 Microwave Sintering

After a review of the basic knowledge on the microwave theory and the interaction mechanism of microwaves and materials, the microwave sintering of materials, especially polymers, is reviewed in this sub-section.

2.1.3.1 Microwave Sintering Overview

Microwave sintering has been well adopted for the processing of metals and ceramics (Oghbaei *et al.*, 2010; Thostenson *et al.*, 1999). The primary advantage of microwave processing is the reduction of processing time. The microwave sintering technique can be divided into direct sintering and hybrid sintering.

Microwave hybrid sintering refers to microwave sintering in which both the materials and external high dielectric loss susceptors are used to absorb the microwave energy.

This method is applicable for materials with low dielectric properties at low temperature. The ability to absorb microwave energy by using the external high dielectric loss susceptors is improved by preheating the materials to a suitably high temperature. Great advantages of microwave hybrid sintering include making otherwise unsuccessful microwave sintering practical, as demonstrated both by simulations and experiments (Janney *et al.*, 1988). Examples of microwave hybrids can been found from the extensive research conducted by the Pennsylvania State University (Anklekar *et al.*, 2001; Cheng *et al.*, 1997; Komarneni *et al.*, 1992). Fully dense metal bodies, including Fe-Ni, Fe-Cu samples, were successfully fabricated by microwave hybrid sintering. Their sintering device consisted of an insulation box inserted with an alumina tube and several SiC/MoSi$_2$ susceptors. A sample was placed in the alumina tube, in which any desired atmosphere, including H$_2$, N$_2$ and Ar, could be introduced.

In microwave direct sintering, the materials themselves act as the only susceptors. The materials couple directly with the microwave. 8 mol% yttria-zironia was processed by microwave direct sintering, for which the required temperature was 300°C lower when compared with conventional sintering in achieving similar densification (Thridandapani *et al.,* 2010). It differs from that in hybrid sintering, in which the microwave field distribution is greatly modified by the presence of susceptors, and the heating source is to some extent moved externally to the sample (Goldstein *et al.*, 1999). The susceptors in hybrid sintering may serve as a shield that keeps the microwave field away from the target sample (Iskander, 1993). In this manner, the microwave sintering time for direct sintering may be reduced as compared with hybrid sintering, which is actually where the great advantage of direct sintering lies. Moreover, direct sintering may be somewhat

easier to conduct, since devices such as insulators and external susceptors, do not need to be designed and manufactured.

In summary, microwave sintering shows great advantages, especially in terms of reducing the processing time and energy, and direct microwave sintering may be somewhat preferred as compared with the hybrid microwave sintering, since it can make full use of the direct-coupling advantages rendered by microwave sintering.

2.1.3.2 Microwave Processing of Polymeric Materials

Early in 1994, research at the National Research Council in the United States suggested that microwave processing showed potential advantages due to its low energy cost. Many studies were subsequently conducted on microwave sintering for ceramics and metal processing (Bykov *et al.*, 2001; Oghbaei *et al.*, 2010; Thostenson *et al.*, 1999).

For polymeric materials, the microwave was adopted for welding and joining (Potente *et al.*, 2002), microwave-assisted synthesis (Wiesbrock *et al.*, 2004), and rubber vulcanization (Krieger, 1992). Several studies were attempted to develop microwave sintering as an alternative to conventional polymeric material processing methods, such as extrusion and compression moulding. The technical barrier may be largely due to the fact that most polymers have low dielectrics, or are transparent to microwaves (Meredith, 1998).

More recent research suggested a solution to overcome this technical barrier. The introduction of high dielectric materials, such as carbon and analogous materials, may

enhance dielectric properties of polymeric materials. Brosseau *et al.* (2001) reported the electromagnetic wave absorbing properties of carbon-black filled PE composites. Kim *et al.* (2009) reported that nanocomposites composed of the CNT, E-glass fabric, as well as epoxy resin can be adopted as electromagnetic wave absorbing layers. The introduction of high dielectric materials can improve the dielectric response of materials under microwave irradiation and allow low-dielectric polymeric materials to be possibly used for microwave sintering.

2.1.4 Conventional and Microwave Processing of Polymeric Materials

In this section, conventional processing techniques for polymeric materials are reviewed. Furthermore, a comparison is made between microwave sintering and the conventional processing techniques.

Composite technology serves as a method to fabricate polymer based composites, resulting in enhanced properties and performance. Here, a review on conventional processing methods is carried out, especially for carbon nanotube (CNT) filled polymeric composites. These methods can be divided into two categories based on their dispersion techniques: solution blending or melt blending.

Solution blending involves dispersion of CNT in the polymer solution by energy agitation, controlled evaporation and final shape forming. A lot of workers have fabricated CNT containing polymer based composites by solution blending. For instance, Li *et al.* (2004) dispersed 10 wt % CNT in ethylene-co-vinyl acetate, with an

observation that the CNT acted as a nucleating agent.

Melt blending is achieved by reducing the viscosity of the polymer matrix by melting and then dispersing the filler into the melted 'gel'. For a thermoplastic polymer which is difficult to dissolve in a solution, melt blending can serve as an alternative to the solution blending method. Based on the technical differences, the melt blending method can be further categorized as extrusion, injection moulding and compression moulding.

Extrusion is an important technique for polymer processing. It has been adopted for polymer based composites such as PP/MWNT composites (Esawi *et al.*, 2010). An extrusion process is carried out by an extruder, which is composed of a driving and a plasticizing system. It has been reported that adopting a screw plasticizing system to plasticize the polymer is fundamentally important (Thomas *et al.*, 2009). A screw plasticizing system is composed of a barrel with one or more screws rotating in the barrel, a heating and cooling unit and some other auxiliary equipment. At the end of the plasticizing system, there is a tool to define the dimensions and shape of the polymer product output. The process of plasticizing is the conversion of a polymer into a plastic state from a solid state, during which the applied heating and forcing are crucial. A single procedure of raising the temperature to the peak temperature in a typical extrusion process takes around 30-120 min (Rauwendaal, 2001).

Injection moulding is another method for manufacturing polymer products. During the injection moulding, a polymer melt is injected into a cold mould, in which the polymer is shaped under the injection pressure. The injection moulding process can be achieved

in two steps: the elementary step and the product shaping step. In the elementary step, transportation of solids, melting, mixing and pressurization are included. In the product shaping step, the polymeric materials are shaped in the mould cavity. In order to inject the polymer into the mould, the melt is pressurized by the forward thrusting of a screw and a piston. The so-called optimal parameters for a given polymer in a given mould cavity are usually obtained by empirical documentation (Tadmor *et al.*, 2006; Thomas *et al.*, 2009).

Compression moulding is also a well known polymer processing technique. It has been used for polymer based composite fabrication, but the thickness of the resultant specimens is typically thin, e.g. a thickness of only 0.5 mm of PP/MWNT composite was fabricated by Logakis *et al.* (2010). In a typical compression moulding process, the polymer in a preformed shape is placed in a heated cavity. Pressure is applied to the polymer while the sample temperature is raised close to the temperature of the mould. There are three procedures in a compression moulding process. Firstly, as the polymer is heated and squeezed, the force rapidly increases. Secondly, the polymer is forced to fill the cavity in a molten state. Finally, the whole polymer melt is compressed and further polymerization reaction takes place. The heat transfer and the elastic deformation are of great importance in the compression moulding process (Tadmor *et al.*, 2006; Thomas *et al.*, 2009).

The conventional polymer processing techniques reviewed above have some limitations. For the solution blending method, contamination may be introduced and some polymers may be difficult to dissolve. For the melt blending method, it involves a conventional

heating process, which is time and energy consuming.

A great reduction in energy consumption and processing time for microwave sintering can be achieved, compared with conventional heating during the heating process. Several studies made comparisons on the specific energy consumption between the microwave and conventional sintering. For processing of silicon nitride based ceramics, 3 kWh kg^{-1} for 2 h was consumed by using microwaves, while 20 kWh kg^{-1} for 12 h was consumed by adopting conventional sintering (Patterson *et al.*, 1992). For the processing of alumina based materials at 1600 ℃, 3.8 kWh kg^{-1} for 60 minutes was consumed using microwave sintering as compared with 58.9 kWh kg^{-1} for 120 minutes using conventional sintering (Patterson *et al.*, 1990). This great reduction in energy consumption in microwave sintering is mainly due to the volumetric heating properties, during which the microwave energy directly couples with the materials and results in rapid heating. For polymeric materials, the conventional processing methods spend great time and energy during the heat conduction and convection (Thomas *et al.*, 2009). Meanwhile, it is expected that microwave sintering can be adopted to reduce the processing time and energy of polymeric materials.

2.2 PP Based Composites and Their Applications

2.2.1 PP Overview

PP is obtained by the polymerization of propylene. There are three types of PP: atactic, syndiotactic and isotactic. These types form under different conditions during the polymerizing process, including the relative orientation of each methyl group and the

degree of polymerization (Pasquini *et al.*, 2005).

Owing to the characteristics including dimensional stability, low density, high chemical resistance, isotactic polypropylene is of high commercial importance. Its industrial applications are in construction, automotive components and fibre manufacturing (Kissel *et al.*, 1999).

In addition to industrial applications, PP has been widely used in biomedical fields, such as abdominal wall hernia repair (Bellón *et al.*, 1998; Campanelli *et al.*, 2008; Cobb *et al.*, 2005; Vrijland *et al.*, 2000), urinary incontinence and prolapsed repair (Cosson *et al.*, 2003; de Tayrac *et al.*, 2007) and tracheal replacement (Behrend *et al.*, 2006; Shi, 2004). The advantages of using PP for tissue replacement include non-biodegradability, durability, high dimensional stability as well as chemical resistivity (Cosson *et al.*, 2003).

In order to modify the characteristics of PP, some particulates (Chiang *et al.*, 1994; Liu *et al.*, 2001; Qiu *et al.*, 2000; Velasco *et al.*, 1996), fibrous fillers (Assouline *et al.*, 2000; Wu *et al.*, 1998) and other polymers (Duvall *et al.*, 1994; Gupta *et al.*, 1984; Ikkala *et al.*, 1993) have been used. With the discovery of CNT, researchers have paid much attention to its composites and applications (Baughman *et al.*, 2002). CNT and PP/CNT composites are reviewed in the following sections.

2.2.2 CNT and PP/CNT Composites

2.2.2.1 CNT Structure and Properties

The structure of CNT is unique. It consists of closed cylinders, which are mainly formed by the strong sp^2 hybridization. The ends of the cylinders may sometimes be capped by hemi-fullerenes. A typical CNT aspect ratio can reach around 1000, as its diameter is at the nanometer scale and length at the micrometer scale (Iijima, 1991; Saito *et al.*, 1998).

The two main CNT types are single-walled carbon nanotubes (SWNTs) and multi-walled carbon nanotubes (MWNTs). SWNTs are composed of one cylinder, while MWNTs are composed of coaxially-arranged cylinders. CNTs can be categorized as: chiral, armchair and zigzag, based on different rolling directions of the graphite tubes. Chiral is termed as non-symmorphic, while armchair and zigzag CNTs are symmorphic. The chiral vector and the chiral angle can be used to describe these structural characteristics (Thostenson *et al.*, 2002).

CNTs have superior electromagnetic absorbing properties. Wadhawan *et al.* (2003) reported that purified SWNTs could be heated to a temperature of 650 ℃ after irradiation for 10 s. Imholt *et al.* (2003) stated that temperature close to 2000 ℃ could be achieved for SWNTs under certain conditions of microwave irradiation. The dielectric properties of CNTs are interesting. Various responses of CNTs to microwave irradiation have also been investigated, such as the light emission, electron spin resonance, and permittivity (Grimes *et al.*, 2000; Petit *et al.*, 1997; Watts *et al.*, 2003).

In addition to the strong electromagnetic absorbing properties, CNTs possess extraordinary mechanical properties. Their strength was reported as ranging from several GPa to as high as 63 GPa (Xie *et al.*, 2000; Yu *et al.*, 2000), with a Young's modulus greater than 1 TPa (Wong *et al.*, 1997).

The review suggested that CNTs could be a promising candidate to act as susceptors in microwave sintering. At the same time, they may also act as a reinforcing phase in a composite system.

2.2.2.2 CNT Composites

The application of CNTs in tissue engineering is a popular research area, for example, sensing, cell behaviour augmentation and matrix enhancement (Harrison *et al.*, 2007). Introducing CNTs as fillers in composite systems might make CNTs safer and more effective in tissue engineering. As a matter of fact, development of both biodegradable and non-biodegradable polymer based composites by the utilization of CNTs has become a popular research topic, though still in its infancy.

Biodegradable polymers were usually incorporated with CNTs in tissue engineering applications, such as poly-L-lactide (PLLA) (Feng *et al.*, 2008; Kim *et al.*, 2008; Zhang *et al.*, 2006), polylactide (PLA) (Chiu *et al.*, 2008; Drumright *et al.*, 2000; Wu *et al.*, 2008b), poly(lactic-co-glycolic acid) (PLGA) (Armentano *et al.*, 2008; Polizu *et al.*, 2006); polycaprolactone (PCL) (Fecek *et al.*, 2008), collagen (MacDonald *et al.*, 2008), and chitosan (Wang *et al.*, 2005). The degradation process was not well covered in the current literature. Moreover, the degradation process of implanted materials could result

in emission of CNTs into the human body, which may be harmful to health.

In addition to the biodegradable polymers, CNTs have also been incorporated into non-biodegradable polymer based composites. PE is well accepted for applications as artificial hips and knees. CNTs were incorporated with PE to improve the physical performance. SWNTs were reported to accelerate the PE crystallization rate (Haggenmueller *et al.*, 2006). PE/MWNT composites were fabricated by melt blending, the percolation threshold of which was found be about 7.5% (McNally *et al.*, 2005). Furthermore, for composites composed of PE-grafted MWNTs and PE, mechanical improvement of stiffness, strength, and retention of toughness was achieved. It was suggested that strong interfacial adhesion between the filler and matrix was induced by the grafting (Yang *et al.*, 2007).

Compared with PE, PP seems to be more suitable as the matrix in the development of biocomposites. PP is a more bio-stable and stiffer non-biodegradable polymer. Compared with PE, less mechanical reduction at high temperatures and better fatigue properties were observed for PP (Liu *et al.*, 2007). The mechanical and thermal properties of PP/CNT composites are reviewed in the section below.

2.2.2.3 PP/CNT Composites

Based on earlier studies, the incorporation of CNTs into the polymer matrix can improve mechanical properties, thermal stability, crystallization behaviour and electrical conductivity (Moniruzzaman *et al.*, 2006; Wiemann *et al.*, 2005). Nucleating effects of PP by incorporating CNTs were reported. Bhattacharyya *et al.* (2003) pointed

out that CNTs act as nucleating sites for PP crystallization, and an addition of 0.8 wt%

SWNT increased the crystallization rate by more than an order of magnitude. Another

study conducted by Valentini *et al.* (2003) showed that there was an increasing

nucleating effect with increasing SWNT loading, which was followed by saturation. As

an indicator of the crystallization effect, the crystallization temperature of a PP matrix

was found to shift to a higher point with increments of CNTs, which was more evident

at lower loadings (Valentini *et al.*, 2003). Regarding the microstructure, MWNTs were

stated to promote the fibrillar morphology in the composites, rather than the spherulitic

morphology in neat PP crystallite, which seemed to be supported by the kinetic data

from differential scanning calorimetry (DSC), according to Ozawa's theory (Ozawa,

1971), that uses a basic nonisothermal crystallization kinetic theory under a constant

cooling rate.

In addition to the nucleating effects in the PP/CNT composites, mechanical

enhancement was also observed. The PP/CNT composite fibres fabricated from solvent

processing and melt spinning increased by 40% in strength and 55 % in modulus, with a

1.0 wt% loading of CNTs (Kearns *et al.*, 2002). Another PP/CNT composite fabricated

from a similar processing approach showed good dispersion and exfoliation. For the

composites, the storage modulus increased by 5 GPa at -140 ℃ and by 1 GPa at 100 ℃,

as compared with controlled pure PP samples. It could be explained by the large

difference in shrinkage between the PP matrix in the PP/CNT composites and the

controlled pure PP (Lee *et al.*, 2008). In composites fabricated by melt blending,

MWNTs were found to be dispersed better in low crystalline PP than in higher

crystalline ones. For a low crystalline PP, 37% improvement of flexural strength was

observed with an addition of 8.0 wt% MWNTs (Liao *et al.*, 2008).

To conclude, CNTs, with strong mechanical properties, have become promising as reinforcing fillers for fabricating polymer based composites.

2.2.3 CNT/HA and PP/HA Composites

2.2.3.1 Structure and Properties of HA

Generally, polymers lack the ability to generate strong bonding with growing tissue, which limits the application of polymers in tissue engineering. Some bioactive ceramics have been introduced to enhance the poor adhesion (Hench, 1998; Misra *et al.*, 2006; Murugan *et al.*, 2005; White *et al.*, 2007).

HA, as a typical bioactive ceramic, has attracted great research interest due to its chemical similarity to the mineral component of bone and other hard tissues in mammals. For natural bone tissue, the main component is calcium phosphate, with a weight percent of 69 wt% (Park *et al.*, 1992). Calcium phosphate bioceramics is actually in the form of crystallized HA and amorphous calcium phosphate.

Pure stoichiometric HA is expressed as $Ca_{10}(PO_4)_6(OH)_2$, which consists of Ca^{2+}, PO_4^{2-}, and OH^- ions. The structure of HA belongs to a hexagonal system with a $P6_3/m$ space group, the overall arrangement of which is characterized by a *c*-axis perpendicular to 3 equivalent *a*-axis at angles of 120° to each other. The atomic arrangement is shown in Fig.2.3 (Shi, 2006).
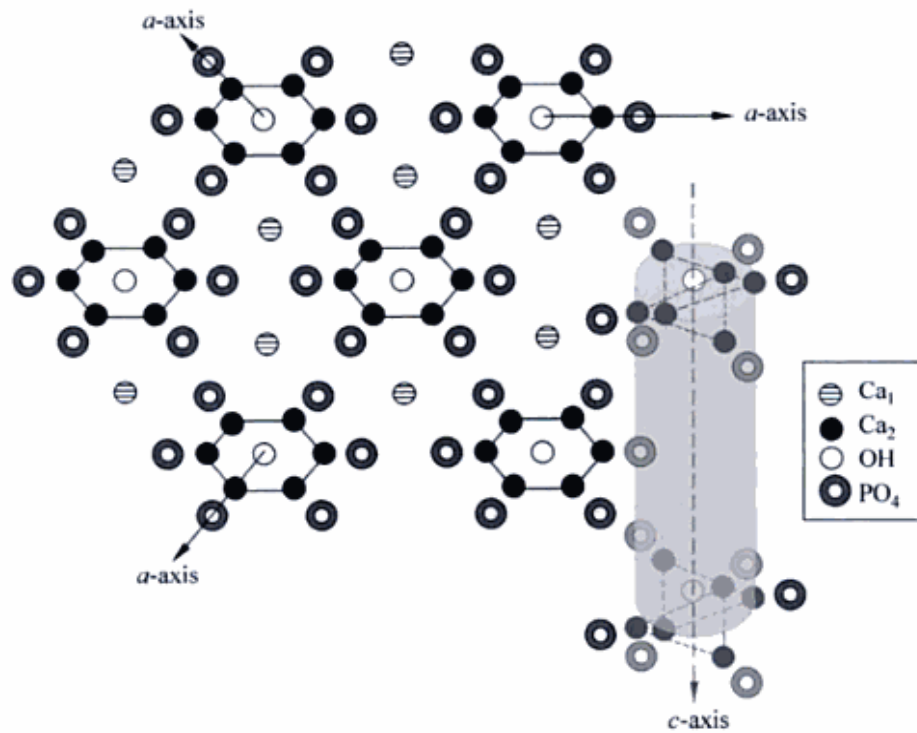
Fig.2.3 Illustration of the atomic arrangement for calcium HA (Shi, 2006)

The biological HA in the body is different from that of pure HA in terms of composition, stoichiometry, mechanical properties and physical properties. The value of the Ca/P ratio in biological HA was reported to be lower than 1.67, the value for pure HA (Harper *et al.*, 1966). Some substitutions are included in biological HA, which may involve ions of Mg^{2+}, Na^+, K^+, Sr^{2+} for Ca^{2+}, Ca^{2+}, CO_3^{2-}, $H_2PO_4^{2-}$, HPO_4^{2-} and SO_4^{2-} for PO_4^{3-}, and F^-, Cl^- and CO_3^{2-} for OH^-, so the appropriate formula of biological HA can be expressed by :

$$(Ca, M)_{10}(PO_4, Y)_6(OH, X)_{2+}$$
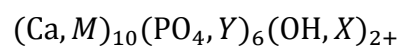
where Mg^{2+}, Na^+, K^+ and Sr^{2+} are denoted as M; Ca^{2+}, CO_3^{2-}, $H_2PO_4^{2-}$, HPO_4^{2-} and SO_4^{2-} are designated as Y; while X represents F^-, Cl^- and CO_3^{2-}.

At the HA-bone interface, stoichiometric HA, with a Ca/P ratio of 1.67, can form a stable carbonated apatite layer, through ion exchange, precipitation and dissolution, strongly characterized as bioactive (Best *et al.*, 1997).

Though possessing attracting bioactivity, the mechanical properties of HA are not suitable for load-bearing applications. HA has a high compressive strength, while it has a significantly low fractural toughness and tensile strength. For dense HA, the compressive strength is about 430-920 MPa (Denissen *et al.*, 1985; Jarcho *et al.*, 1976; With *et al.*, 1981), while it is 100-230 MPa for cortical bone and 2-12 MPa for cancellous bone (Hench *et al.*, 1993). The tensile strength for dense HA is 17-110 MPa (Denissen *et al.*, 1985; Jarcho *et al.*, 1976), which is higher than the 10-20 MPa for cancellous bone, but lower than the 50-150 MPa for cortical bone. The fracture toughness of HA is no more than 1 MPa $m^{1/2}$ (Denissen *et al.*, 1985; Jarcho *et al.*, 1976), which is much lower than the 2-12 MPa $m^{1/2}$ for cortical bone. In other words, HA may not meet the mechanical requirements for natural bone replacement.

In order to circumvent its mechanical weakness, and at the same time to utilize the bioactive property, some researchers have developed a HA-based coating on load-bearing metals, such as titanium, for implantation (Chen *et al.*, 2005; Khor *et al.*, 2000; Lynn *et al.*, 2002). However, the bonding strength between the calcium phosphate layer and the titanium alloy surface was sometimes weak (Chen *et al.*, 2006; Porter *et al.*,

2004), either due to the formation of Ca-Ti-Oxide layers of several micrometer thickness (Gross *et al.*, 1998), or due to the uncontrolled dissolution of the HA layer (Zeng *et al.*, 2000). Researchers have been trying to find some other ways to solve this problem. Design of polymer based composites with a balance of the mechanical and biological properties has become a popular research topic.

2.2.3.2 CNT/HA Composites

As a coating material for high-load-bearing metal implants, CNT/HA composites have been fabricated through laser surface alloying, with a 43 % increment in hardness and a 21 % increment in Young's modulus, compared with a single phase HA (Chen *et al.*, 2006). By using electrophoretic deposition, MWNT reinforced HA composites have been coated on a Ti-6Al-4V implant, for which up to 300 % improvement of inter-laminar shear strength over the monolithic HA was observed (Kaya, 2008).

In addition to act as coating materials, CNT/HA composites have been studied as direct-load-bearing materials. Greater than ten percent increments in compressive strength have been reported for HA based MWNT composites by in-situ synthesis (Zhao *et al.*, 2004). Kealley *et al.* (2008) fabricated high-densified CNT/HA composites with high hardness but low fracture toughness.

As a matter of fact, there has been little research reported in the current literature for the fabrication of solid structures made by CNT/HA composites (Meng *et al.*, 2008), probably due to the difficulty in the processing of the HA matrix. Moreover, the reported mechanical improvements were limited to hardness, stiffness and compressive

strength. It would be a break-through if polymers could be introduced to improve the toughness as well as processability of HA (Hatzikiriakos *et al.*, 2005).

2.2.3.3 HA/PP and HA/PE Composites

PE and PP have been incorporated with HA for composite fabrication. By modifying high-density PE with HA, HAPEX^{TM} has been developed as a commercial product. Its tailored stiffness, toughness and bioactivity, make it suitable for low load bearing implantation. Compared with PE, PP appears to be more suitable as a matrix. PP exhibits better fatigue performance and maintains stable mechanical properties at high temperatures (Liu *et al.*, 2007).

HA particles can stiffen the composite, and increase the modulus. As shown in Table 2.1, the moduli are summarized for HA/PP, HAPEX^{TM} (Liu *et al.*, 2007; Shi, 2004), as well as for natural bone (Wang *et al.*, 2000).

HAPEX^{TM} has been used successfully for clinical orbital floor and middle ear prosthetic implants (Downes *et al.*, 1991; Tanner *et al.*, 1994). Young's moduli of HA/PP composites are higher than those of HAPEX^{TM}, both of which have an increasing trend with increasing HA volume fraction. HA/PP is stiffer and stronger than HA/PE, which suggests applications for higher load bearing tissue implants.

HA has the ability to stiffen composites, and increase their moduli. The properties of the composites might be influenced by the HA amount introduced in the composites. Nowadays, volume fractions of the HA filler in HAPEX^{TM} achieved 45 vol % when

fabricated by a method which consists of mixing, milling and compounding, followed by compression moulding and injection moulding (Wang *et al.*, 2000; Zhang *et al.*, 2003). However, the maximum volume fraction of the HA filler in HA/PP composites was only 25 vol % by injection moulding (Liu *et al.*, 2007). A new processing method needs to be developed to fabricate HA/PP composites with a higher HA filler volume fraction.

Table 2.1 Elastic modulus of HA/PP composite, HAPEX^{TM} and natural bone

Materials			**Elastic Modulus** (GPa)
HA Volume percent (%):	0	HA/PP	1.3
		HAPEX^{TM}	0.65
	10	HA/PP	2.2
		HAPEX^{TM}	0.98
	20	HA/PP	2.6
		HAPEX^{TM}	1.60
Cancellous Bone			0.05-0.5
Articular Cartilage			0.001-0.01
Tendon			1
Cortical Bone			7-30

2.2.4 Summary for the PP Based Composites

The introduction of carbon nanotubes (CNTs) as nanophase fillers has achieved great success due to their outstanding mechanical properties and unique morphology (Coleman *et al.*, 2006). By incorporating with CNTs, PP shows advantages in improved

Young's modulus and flexural strength.

HA, as a bioactive ceramic, has a strong ability to form a stable carbonated apatite bond at the HA-bone interface. CNT/HA and HA/polymer composites have been designed and fabricated with a certain degree of success. For HA/polymer composites, including HA/PE and HA/PP, it is preferable if strong fillers could be introduced for strengthening (Wang *et al.*, 2000; Zhang *et al.*, 2003).

The above review suggests a way in which combining the advantages of HA, CNT and PP may improve the composite performance. In this study, the fabrication of PP/CNT/HA composites is explored.

2.3 Methods for Dispersion and Blending

Among several important factors in the fabrication of CNT/polymer composites, the dispersion problem is a critical one. Thostenson *et al.* (2002) pointed out that the uniform dispersion of CNTs within the polymer matrix is critical in the processing of polymer based CNT composites. Only when CNTs are uniformly dispersed and exfoliated in the matrix, can forces be efficiently transferred in the composites. In this section, the methods for dispersion and blending of polymer based CNT composites are reviewed in terms of the solution blending and melt blending based methods.

2.3.1 Solution Blending Method

The solution blending method aims to make a better dispersion of the CNT fillers within the matrix in solution form. Various energy agitation approaches have been adapted for dispersion in solution: mechanical stirring, ultrasonication, magnetic field alignment and spin casting.

Sandler *et al.* (1999) presented a typical procedure for solution blending, by taking the fabrication of epoxy/CNT composites as an example with the following steps: (1) disperse CNTs in ethanol solution by mechanical stirring (2) add epoxy resin and keep stirring (3) add additives (*e.g.* to harden) and continue stirring (4) dry the mixture. A composite fabricated from this process showed improvement in overall electric conductivity, however, the CNTs were not uniformly dispersed at the millimetre scale.

In the ultrasonication method, CNTs are dispersed in solution by ultrasonic waves. The advantage of ultrasonication is its ability to break the CNT entanglements. Qian *et al.* (2000) fabricated polystyrene/CNT composites in the following procedures: (1) disperse MWNTs and polystyrene (PS) in toluene solution separately by high energy ultrasonication (2) mix these two solutions together in a continued ultrasonication bath (3) cast the mixture into a culture, allowing toluene to evaporate. The incorporation of only 1 wt% CNTs resulted in several ten percent increments, both in elastic modulus and in breaking stress, indicating good dispersion and an efficient CNT load transfer.

Magnetic field assisted dispersion is another commonly adopted method, which typically aims to obtain a good alignment of CNTs in the polymer matrix rather than a

random dispersion. Kimura *et al.* (2002) fabricated polyester based composites with good CNT alignment, by applying a constant magnetic field of 10 T in a mixture of unsaturated polyester styrene monomers and CNTs. Through a combination of hot-pressing and magnetic alignment, Takahashi *et al.* (2003) obtained well aligned carbon fibres in a polycarbonate matrix, which was confirmed by X-Ray diffraction and magneto-mechanical theory. It was suggested that the magnetic field mechanism assisted the alignment. Since the parallel diamagnetic susceptibility was smaller than that in the perpendicular direction, CNTs tended to align parallel to the magnetic field by overcoming the thermal energy. The resulting alignment enhanced the electrical conductivity and elastic modulus in a particular direction. However, the agglomeration of CNTs is a typical problem when using this magnetic assisted method (Takahashi, 2003).

Another solution blending technique is the spin casting method. Safadi *et al.* (2002) processed polystyrene based CNT composites via spin casting. The general procedures are as follows: (1) mix the polymer matrix and CNTs (2) deposit the mixture at the centre of a rotating disk. The obtained alignment of the fillers within the samples was characterized as parallel to the radial direction near the disk centre and perpendicular to the radial direction near the edge of the disk.

After the above review regarding solution blending based dispersion, the following conclusions can be drawn: for better dispersion, the ultrasonication method is better than mechanical stirring, while the dispersion effect from their combination may be rather significant; for better alignment, the magnetic field method is successful to some

extent apart from the CNT agglomeration problem, while the disadvantage of spin casting lies in the different CNT alignment directions at various locations within the resulting sample.

2.3.2 Melt Blending Method

In this section, the melt blending method is reviewed, two general types of which are solution based melt blending and direct melt blending.

The solution based melt blending method is to melt and stretch mixtures, which are being dried from solution. Cooper *et al.* (2002) used a German made Molinex Attritor to mix the composites right after the ultrasonication and drying from solution. Haggenmueller *et al.* (2000) folded and hot pressed the as-cast solution based composites, and drew them into different ratios.

Direct melt blending melts and stretches directly without pre-dispersion in a solution form. Thostenson *et al.* (2002) used a micro-scale twin screw extruder and a hydraulic press to randomly orient the CNTs. Bhattacharyya *et al.* (2003) used a mixer to fabricate the composites directly.

While achieving a certain degree of success, both melt blending based methods involve melting procedures, which consume much energy and time. Moreover, they are not applicable for thermosetting polymers.

2.4 Theoretical Approaches to Simulate Mechanical Properties of Porous Composites

Porous composite materials can be regarded as materials consisting of different phases, one of which is void. In this manner, the review on the theoretical approach to simulate the mechanical properties of porous composites is actually that of the common multi-phase composites. For multi-phase composites, most analytical models are based on a number of basic ones.

Some basic analytical models for multiphase materials are reviewed. The simplest two are the Voigt and the Reuss models, which provide the upper and lower bounds by considering the arithmetic and harmonic average of the elastic moduli (Wong *et al.* 1999). Ishai and Cohen (1967) proposed a method for elastic modulus prediction, when assuming uniform displacement being applied at composites with macroscopically homogeneous stress and with maintained interface adhesion. This model generally underestimates the elastic modulus (Liang *et al.,* 1997). The modified Kerner equation and the Hashin and Shtrikman model can estimate moduli close to experimental results. The Kerner equation was derived by Kerner (1956), and estimates the elastic modulus of composites, in which the fillers are much stiffer than the matrix. The Kerner equation was modified by Nielsen (1970), by taking into account the particle packing density. The modified Kerner equation assumes the particles are macroscopically homogeneously distributed and are perfectly bonded with the matrix. The Hashin and Shtrikman model was developed to estimate the composite elastic modulus (Hashin *et al.,* 1963). In their model, the Poisson's ratio of each phase was taken into consideration.

While acceptable predictions can be obtained by the basic models, measurements are needed to improve their applicability and accuracy. Some may include combinations of two or more basic models (Wang *et al.,* 2008).

2.5 Limitations and Technology Barriers

Recently, microwave processing of materials has received more research interest (Bykov *et al.*, 2001; Oghbaei *et al.*, 2010; Thostenson *et al.*, 1999) due to the advantages of reduced processing energy and time by direct coupling with microwaves (Thostenson *et al.*, 1999), and a high bonding strength between the filler and the matrix (Wang *et al.*, 2007).

Currently, research has been conducted to explore the application of microwaves in the fabrication of polymer based composites. The current gap is mainly due to microwave transparency or the low dielectric loss constants of most polymers. CNTs possess great electromagnetic absorbing properties (Mendez *et al.*, 2003; Wang *et al.*, 2007), as well as unique mechanical (Iijima, 1991; Saito *et al.*, 1998) and morphological characteristics (Thostenson *et al.*, 2002). In this study, CNTs are introduced as susceptors in the microwave processing of microwave-transparent polymers.

The homogenous dispersion of particles, especially CNTs, is critical. Nano-sized CNTs tend to agglomerate due to their high surface energy. The agglomeration of CNTs results in non-uniform energy adsorption and low load transfer efficiency. More

severely, it would end up with severe cracks within the samples due to the non-uniform heating. Developing appropriate methods to achieve a homogenous dispersion of the CNT particles in the composite fabrication is essential.

In addition to the dispersion problem, the non-uniform distribution of the microwave field may also be a challenge in microwave sintering. Both single and multi-excitation mode microwave applicators result in non-uniform magnetic fields, in terms of "hot spots" and their overlapping. The non-uniform field distribution renders the non-uniform heating of materials, which may also result in cracks within the materials.

Chapter 3: Fabrication and Characterization of PP/CNT/HA Composites

3.1 Fabrication of PP/CNT/HA Composites

In this section, the fabrication process of the PP/CNT/HA composite is described systematically. With details of the raw materials given, the composite fabrication process is explained in terms of powder dispersion, compaction, and finally microwave sintering.

3.1.1 Raw Materials

PP was selected as the matrix for composite fabrication by microwave sintering in this study. The PP powder was obtained from Goonvean Fibres (Devon, UK), with a density of 0.9 g cm^{-3} and particle sizes ranging from 50 to 80 μm. The melting point was in the range of 150-170 $^{\circ}$C. Multi-walled carbon nanotubes (MWCNTs) (catalog no. S-MWNT-1020) were purchased from the Shenzhen Nano-Tech Port Co., Ltd. (Shenzhen, China). The purity of the CNTs was > 95%. The outer diameter was 10-20 nm and the length 5-15 μm. The as-received CNTs were immersed in 38 % hydrochloric acid for 24 hours for purification, which was followed by washing with de-ionized water to pH=7.0.

Nano-sized HA was introduced with different compositions. The HA was obtained from Kingo Advanced Materials R&D Co., Ltd. (Ningbo, China). The nano-sized HA was

irregular-plate-shaped, with a length in the longest direction of 400 to 2000 nm.

3.1.2 Powder Dispersion

The dispersion problem of CNTs in the PP/HA blend has to be solved. In the PP/CNT/HA composite system, non-uniform CNT dispersion may result in heat concentration, deformation and probably cracking within the samples. Moreover, non-uniform dispersion can cause an inefficient force transfer at the filler-matrix interface in the composites (Thostenson *et al.*, 2002).

Based on the literature review given in the previous chapter, a combination of ultrasonication and mechanical stirring in a solution based condition was proposed to uniformly disperse the CNTs. The adopted polymer, PP, is insoluble (Maier *et al.*, 1998) so that de-ionized water and ethanol were used to form a suspension. Within this suspension system, the PP particles were at the micro-scale while the CNT and HA were at the nano-scale.

A series of steps for the powder dispersion process was adopted: (1) the three types of particles were ultrasonicated in de-ionized water or ethanol suspension respectively (2) the separated suspensions were mixed by combined ultrasonication and stirring (3) the mixed suspension was dispersed by continuous stirring. A schematic diagram with detailed parameters for these procedures is shown in Fig.3.1. Actually, much work was conducted in deriving the actual operational sequence. Firstly, a combination of ultrasonication and mechanical stirring was determined as the dispersion technique,

based on the literature review, during which ranges for various parameters were found. Secondly, a preliminary study was carried out to examine the morphology of the samples when fabricated with various well-designed parameter values within each range. One of the important parameters was the ratio of CNTs to distilled water during the first ultrasonication procedure, as large ratios showed non-uniform dispersion in terms of the large deformation of the samples during sintering. Eventually, final procedures with detailed parameters values were designed as shown in Fig.3.1.
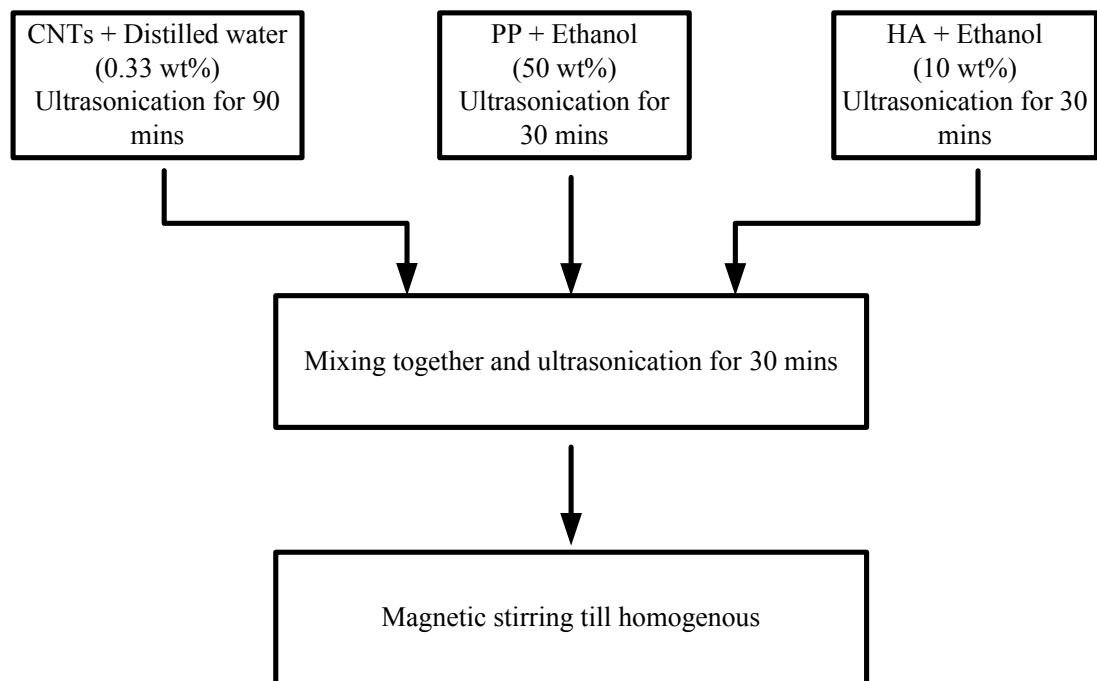
Fig.3.1 Schematic diagram for the procedures of powder dispersion

During the first step, the de-ionized water suspension for CNTs should be diluted sufficiently so as to allow each CNT to occupy its own space after being disentangled by ultrasonication. Preliminary results indicated that a 0.33 wt% CNT-water suspension resulted in satisfactory dispersion results. Meanwhile, PP and HA were ultrasonicated in

ethanol at 50 wt% and 10 wt%, respectively. In the current study, an ultrasonicator (CP 2600, Crest Ultrasonic Powersonic), with an average power of 300 W and a frequency of approximate 45 kHz, was adopted. The ultrasonication time for each of the suspensions was set based on dispersion conditions of preliminary attempts.

During the second step, the three suspensions were mixed by combined ultrasonication and stirring. The stirring was carried out by a magnetic stirrer (SP18420, Nuova Stir Plate). The purpose was to largely avoid the re-agglomeration of the disentangled CNTs. The time period for this procedure was set at 30 minutes.

In the final stage of the powder dispersion process, stirring by the magnetic stirrer was carried out until homogenous dispersion was achieved. During the stirring, the CNTs and HAs could be attached to the surfaces of the PP particles, due to the high surface energy of the nano-particles. Since the mixed suspension was diluted, the disentangled CNTs could be attached little-by-little during stirring. This kind of process might produce a resultant homogenous dispersion.

3.1.3 Powder Compaction

The well-dispersed mixtures were dried for further compaction. The relative compaction density of the green compact should be high for the sintering high density sample (German, 1996). Here, the powder compaction can be divided into four steps: powder sieving, mould lubrication, particle rearrangement and powder pressing, as shown in Fig. 3.2.

```
┌─────────────────┐      ┌─────────────────┐      ┌─────────────────┐      ┌─────────────────┐
│                 │      │                 │      │    Particle     │      │                 │
│  Powder Sieving │ ───▶ │ Mould Lubrication│ ───▶│  Rearrangement  │ ───▶ │ Powder Pressing │
│                 │      │                 │      │                 │      │                 │
└─────────────────┘      └─────────────────┘      └─────────────────┘      └─────────────────┘
```
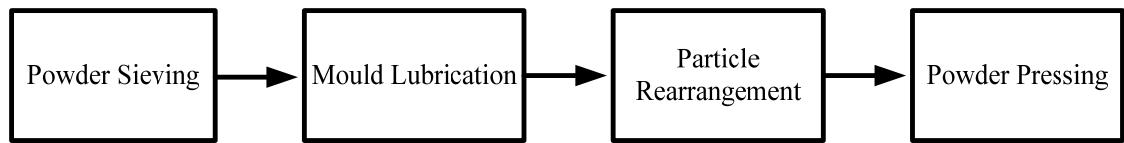
Fig.3.2 Flow diagram for procedures of the powder compaction

The powder sieving procedure was to narrow down the range of the particle size distribution. The logic of this procedure was based on the conclusion that a narrower distribution of particle sizes gives rise to a higher green compact density (German, 1989). The particles tend to agglomerate after drying from the suspension. The resulting agglomerates may vary in size, and may be much larger than the 50-80 μm of the as-received PP particles, which widens the distribution range of the particle sizes. In the powder sieving procedure, the particles were sieved by a sieve with opening sizes of 75-120 μm in diameter. During sieving, most agglomerates were manually broken down to the original particles, so that they could go through the sieve opening. In this manner, the distribution range of particle sizes was narrowed.

The objective of the mould lubrication procedure was to reduce the friction force between the mould and the green compact. Several studies have been conducted to lubricate the mould by using various lubricants, which was proved to effectively reduce the friction force (Cannon *et al.*, 1989; Rahman *et al.*, 2009; Taniguchi *et al.*, 2005). The frictional force has detrimental effects on the quality of the green compacts, by introducing a non-uniformly distributed stress field, with cracks both on the surface and within the bulk. In this study, the mould cavity was highly polished to reduce the frictional force.

After being pasted with the lubricant, the powder was added to the mould for compaction. The mould was 20.0 mm in diameter. Particle rearrangement was a procedure prior to the formal compaction, which aimed at rearranging the loosely arrayed particles to a closer packing, thus improving the density of the green compact. It was achieved by applying a small dynamic load, i.e., a pressure less than 0.05 MPa (German, 1989). In this study, a 1 Hz sinusoidal load was applied for particle rearrangement, with the lowest and highest values of 10 N and 20 N, respectively.

After particle rearrangement, the formal compaction, i.e. powder pressing, was conducted. The compacting cycle consisted of the following three steps: (1) elastic deformation (2) massive deformation throughout for all particles, and (3) full compaction in the whole bulk (German, 1989). A peak load of 40 kN, i.e., 127 MPa, was adopted in order to enable the PP particles to go through plastic deformation. Moreover, a holding time of 200 s at the peak load was adopted, which could further aid compaction of the deformed powder in the whole bulk. In addition to the loading parameters, another important parameter was the thickness-to-diameter ratio of the green compact. It was reported that a smaller ratio of thickness to diameter resulted in a more uniform stress distribution along the depth direction within the sample (German, 1989). In this study, the diameter and the thickness of the green compacts were about 20 mm and 3 mm, respectively.

3.1.4 Sintering Process

Microwave direct sintering was used in the current study. A domestic microwave oven

(1100 W, NN-ST557M, Panasonic) was used for sintering the composites at full power, as shown in Fig.3.3. A microwave-transparent ceramic disk was used to hold a sample during sintering. Four compositions, PP (wt %):CNT (wt %):HA (wt %), equal to 100:1:0, 100:1:5, 100:1:15 and 100:1:30, were sintered. Only 1 wt% CNT composites were investigated in the current study, as this composition was suggested to result in good morphology after sintering, based on the preliminary study results.

Fig.3.3 Image of the microwave oven for composite sintering used in this study

An image of the successfully sintered PP/CNT/HA (100:1:5 wt %) sample is shown in Fig. 3.4.

Fig.3.4 Image of the sintered (100:1:5 wt %) sample

As a matter of fact, the non-uniform microwave field distribution is a typical problem. For the multi-mode magnetron used in this study, the microwave field distribution is non-uniform. Many studies have been conducted to solve the microwave distribution problem that exists in microwave ovens. Some studies adopted hybrid sintering to obtain a uniform heating, in which susceptors and insulators were introduced to modify the heat distribution (Anklekar *et al.*, 2001; Cheng *et al.*, 1997; Komarneni *et al.*, 1992). However, it is difficult to make full use of the advantages of microwaves, such as direct coupling with materials (Goldstein *et al.*, 1999). Some other studies include the application of a rotating disc, which is typical in most domestic microwave ovens. The microwave field distribution may change with the position movement of the sample (Lidström *et al.*, 2001). The complexity of the microwave field distribution cannot ensure a uniform microwave distribution by using a rotating disc.

In the current research, microwave field distribution rather than the frequency variation seems to more significantly influence the sample quality. Therefore, measurements were taken focusing on the microwave distribution effect. In a microwave oven, there are typically three to six different modes of heating, which provide areas of either high or low field strength (Lidström *et al.*, 2001). It is expected that a specific area could be found in the oven, within which the microwave strength is comparatively high and uniform. Here, such an area was identified and each of the samples was placed in this location for microwave sintering, with less than a 1.0 mm distance deviation. Attempts were made to look for a position in the oven where the specimen can absorb consistent power from the microwave, rather than to look for a uniform field. After sintering, both

the oven cavity and the dish were cooled down to room temperature before sintering the next sample. The reason is that magnetrons are designed to reduce their output power when the cavity temperature is high, as a protection mechanism (Lidström *et al.*, 2001).

3.1.5 Fabrication of PP/CNT/HA Composites with 10%, 30% and 50 vol % of HA

A further attempt to fabricate the composites with higher HA volume percentages was made by using the proposed method. The composite fabrication process was applied to the preparation of the composites with high HA volume percentages (10%, 30% and 50 vol %). The preparation method was the same as in the previous sections. PP with up to 50 vol% HA filling was successfully fabricated by microwave technology. The PP/CNT/HA composites with 10%, 30% and 50 vol % are shown in Fig. 3.5. The successful fabrication of the PP/CNT/HA composites suggests that the method developed in this study, combining powder dispersion, compaction, and microwave sintering, can be an alternative method to fabricate PP/CNT/HA composites with high HA filling ratios. The HA filling ratio was higher than some other conventional processing techniques such as injection moulding, with the highest HA filling ratio of 25 vol % (Liu *et al.*, 2007). This composite fabrication technology may be applied to fabricate some other polymer base composites with high HA filling ratios.
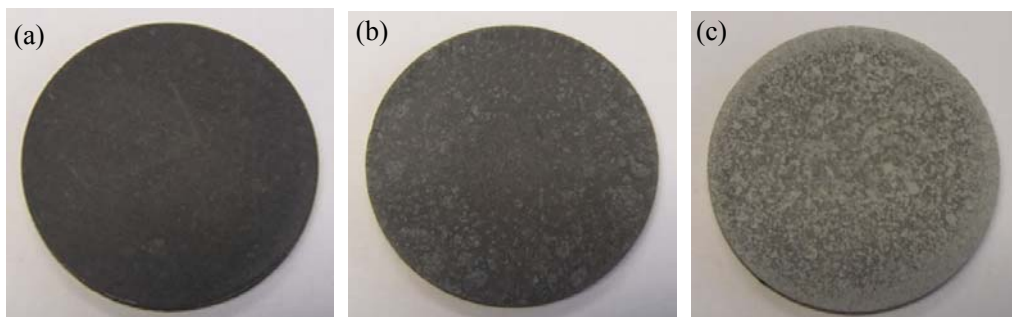
Fig.3.5 Images of the fabricated PP/CNT/HA composites with (a) 10%, (b) 30% and (c)

50% volume percentage of HA

3.2 Characterization of PP/CNT/HA Composites

3.2.1 Sintering Time

The duration of microwave irradiation for each composition is presented, as shown in Table 3.1. The sintering time for each sample was determined by examining the surface morphology of the sintered specimens. The samples were sintered into the whole bulk rather than the originally separated particles, with no sign of over-sintering, i.e., decomposition, observed. The determined sintering is reasonably considered as optimal based on these observations. The resulting morphology and composition is presented in the following XRD and SEM characterization.

Table 3.1 The sintering time for the microwave sintered composites

Samples [PP:CNT:HA (wt%)]	100:1:0	100:1:5	100:1:15	100:1:30
Sintering time (s)	50	25	23	22

The sintering time is reduced to less than a minute, with the addition of the CNT and HA. This is a significant reduction in heating time, as compared with conventional polymer processing methods. Taking a typical extrusion process as an example, 30-120 minutes are needed in the single procedure of heating materials to the peak temperature (Rauwendaal, 2001). Another interesting finding is the trend of the sintering time, which decreases with increase of HA content, probably due to the relative reduction of

the microwave transparency of PP.

3.2.2 Composition Characterization

Over-sintering may lead to decomposition of PPs. Composition characterization was carried out to investigate the phase change of PP after sintering. The sintered samples were examined by X-ray Diffractometer (XRD, Bruker D8 Discover), in which a ray of 0.1542 nm wavelength radiated from Nickel-filtered Cu was directed to the samples. The XRD patterns were scanned with 2 theta ranging from 10 to 55 degrees at a rate of 1 degree min^{-1}. XRD patterns of microwave sintered composites are indexed as shown in Fig.3.6. It can be concluded that the microwave sintering did not cause any PP and HA phase transition.
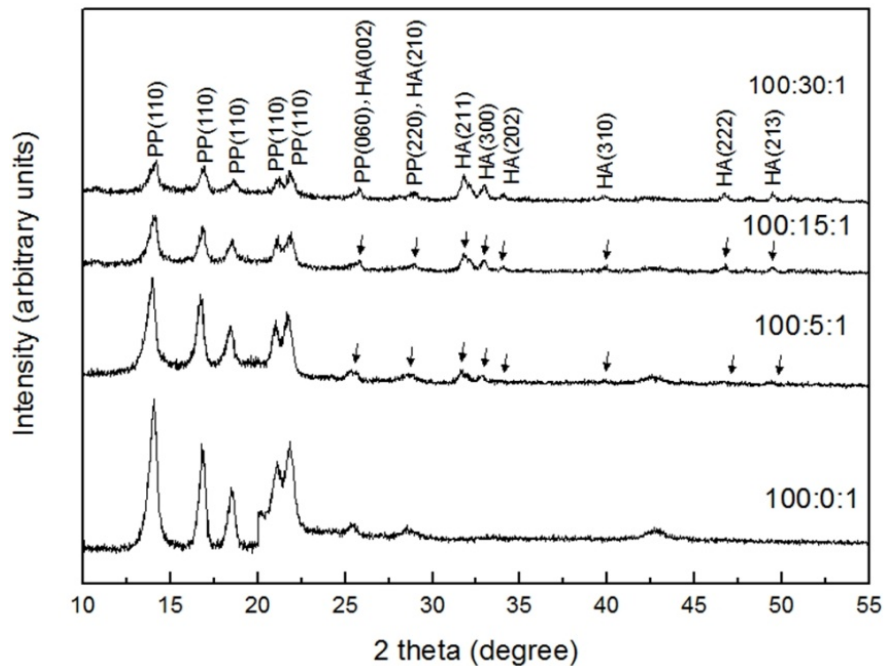
Fig.3.6 XRD patterns of the microwave sintered composites

3.2.3 Microstructure Observation

After confirming the PP and HA composition in the sintered samples by XRD experiments, the following work was conducted to examine the HA distribution within the sintered composites, and the morphology of the microstructure at high magnification. Furthermore, the porosity was investigated.

3.2.3.1 HA Distribution

Back scattered scanning electron microscopy (BS-SEM, Jeol JSM-6490) was used to examine the polished surfaces of the samples. Samples of 2~3 mm thickness were placed on a stub and coated with carbon. The examination was conducted at 20 kV. The BS-SEM micrographs of the microwave sintered samples are shown in Fig.3.7.
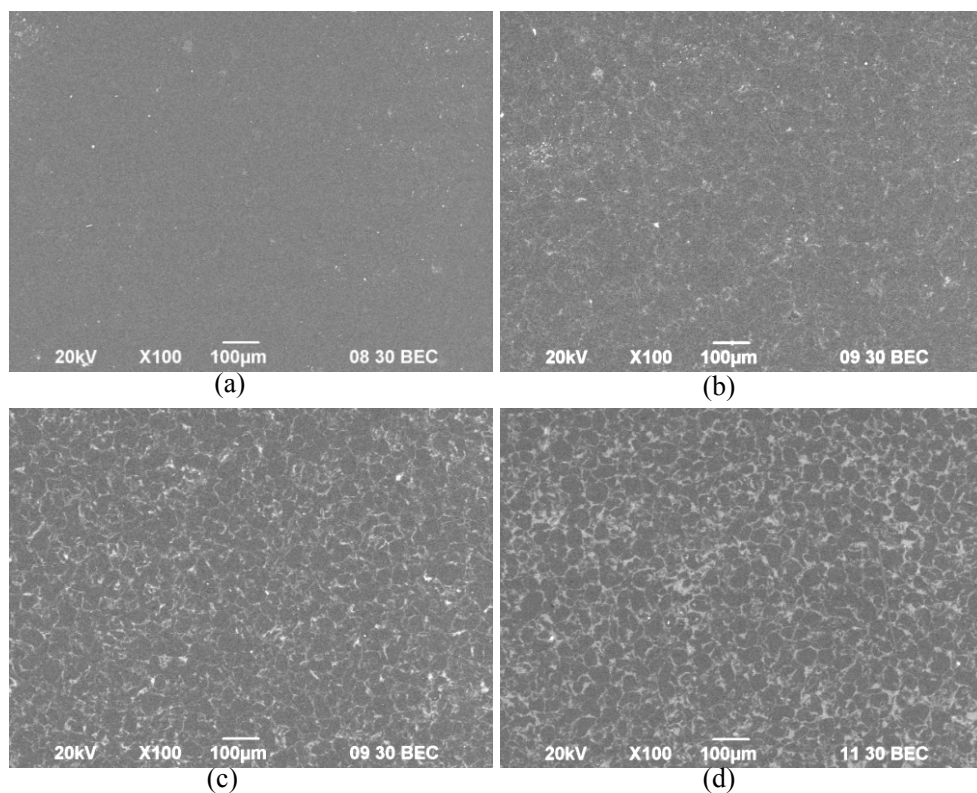
Fig.3.7 BS-SEM micrographs of polished surfaces of sintered PP/CNT/HA composites:
(a) 100:1:0, (b) 100:1:5, (c) 100:1:15 and (d) 100:1:30

In Figs.3.7(b-d), the evident white colour is observed in the micrographs with HA compositions. In order to confirm the composition of the white-coloured areas, EDX examination was conducted. The EDX test result for the composite 100:1:30 is shown in Fig.3.8.
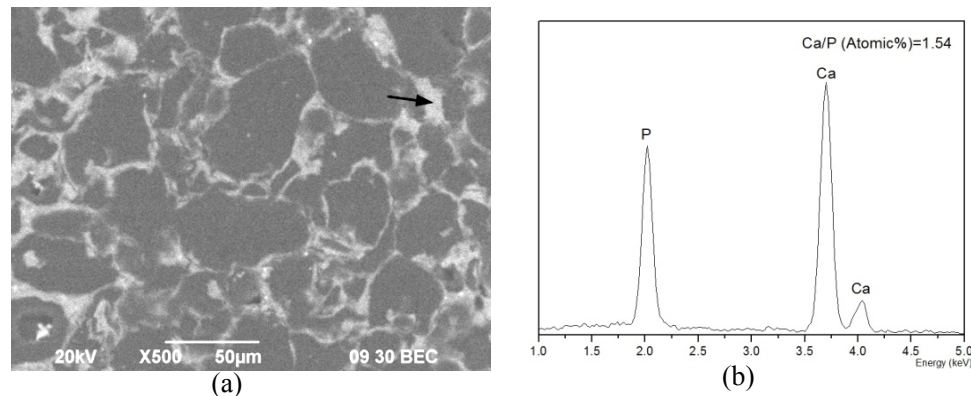
Fig.3.8 (a) Magnified BS-SEM micrograph of polished surface of 100:1:30, (b) EDX spectra of the area in micrograph (a) as pointed by the arrow

As shown in Fig.3.8, it can be concluded that the white colour represents the HA, since the spectra in Fig.3.7(b) indicates that the atomic ratio of Ca/P is 1.54, which is close to 1.67, the claimed ratio for HA.

As shown in the BS-SEM micrographs from 100:1:5 to 100:1:30 in Figs.3.6(b-d), the HA particles, as represented by the white colour, are uniformly distributed. Further examination reveals that the PP matrix is uniformly filled by the HA particles, which can be explained by the dispersion process with the nanophase particles being attached onto the surface of the PP particles.

3.2.3.2 Microstructure at High Magnification

Field emission scanning electron microscopy (FE-SEM Jeol JSM-6335F) was adopted to examine the fracture surfaces of the microwave sintered samples, in which the morphology of the CNTs may be observed.

(a) (b) (c) (d) (e)
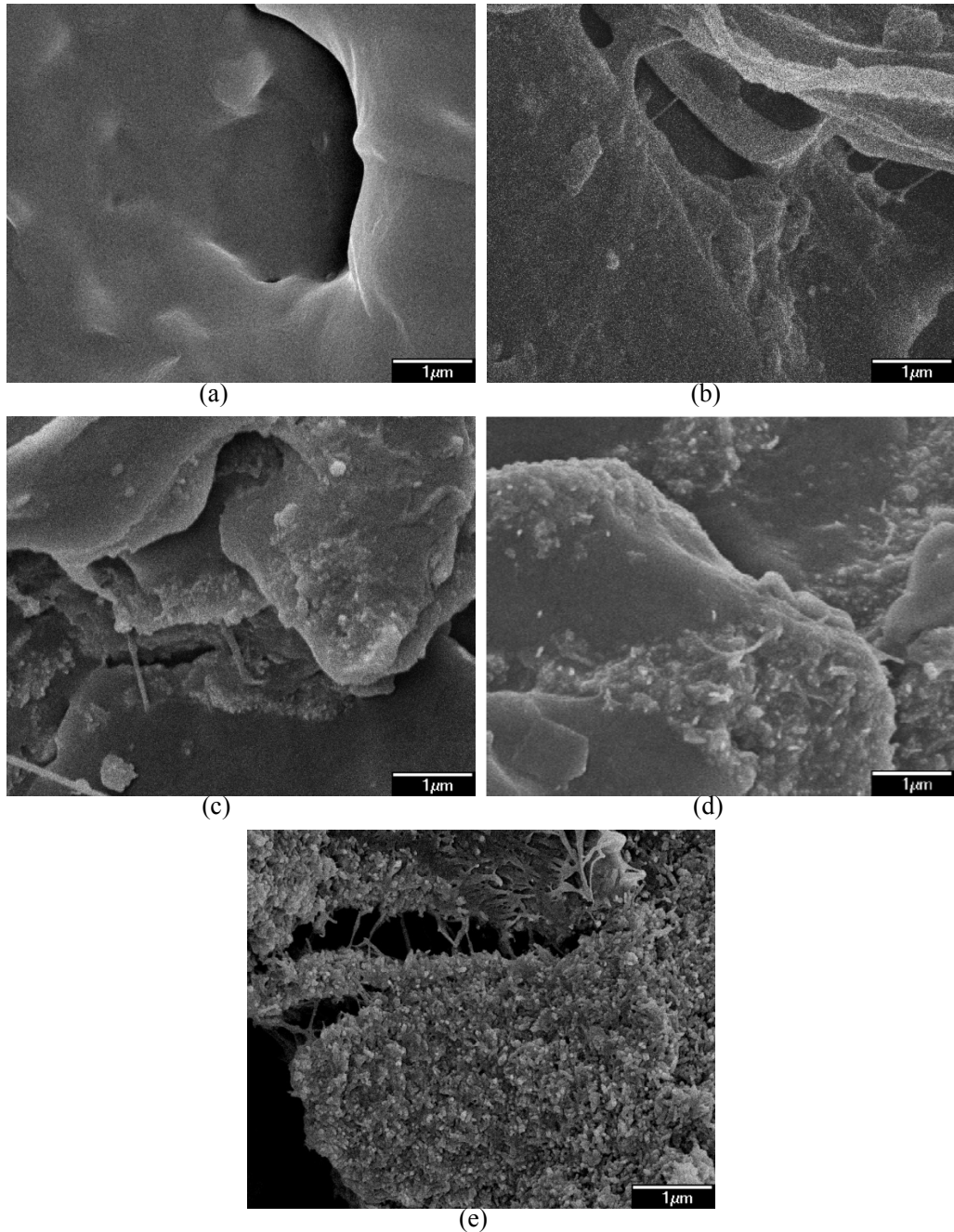
Fig.3.9 FE-SEM micrographs of the fractured surfaces: (a) pure PP, sintered PP/CNT/HA composites of (b) 100:1:0, (c) 100:1:5, (d) 100:1:15 and (e) 100:1:30.

The samples were fractured after being immersed in liquid nitrogen for cooling, which enabled ductile-brittle-transition of the PP matrix and thus brittle fracture (Wang *et al.* 2002). The brittle fracture was made possible to examine the intact morphology of the microstructure within the samples. Therefore, phenomenon such as the bridging effect, could be observed and analyzed. Samples with thicknesses 2~3 mm were placed on a stub and coated with gold. The observation was carried out at 5.0 kV. For comparison, unmodified PP plates (Changzhou No.3 Plastic Co., Ltd., China) fabricated from extrusion moulding were used as controls.

In Fig.3.9, unmodified PP shows a smooth surface. The crack bridging effect is observed at the fracture site for all the PP/CNT/HA composites. The bridging elements are probably due to the breakage of the sintered PP. Similar images suggesting the mechanical enhancement effect can be found in the literature (Coleman *et al.*, 2006). The roughness extent of the fracture surfaces increases from Fig.3.9 (b) to (e). It is assumed that the roughness of the surfaces is due to the agglomeration of the HA particles, while further characterization should be carried out for validation.

3.2.3.3 Morphology of Pores

Porosity is one of the key factors that influence the mechanical performance of materials fabricated by sintering (German, 1996; Olevsky, 1998). The morphology of pores on the fracture surfaces of the microwave sintered samples was examined by secondary electron imaging using scanning electron microscopy (SEI-SEM Jeol JSM-

6490). 20 kV was selected as the observation voltage. The samples were also fractured in a brittle mode by being treated with liquid nitrogen, which could keep the morphology of pores unchanged after fracture. The images produced are presented in Fig.3.10.
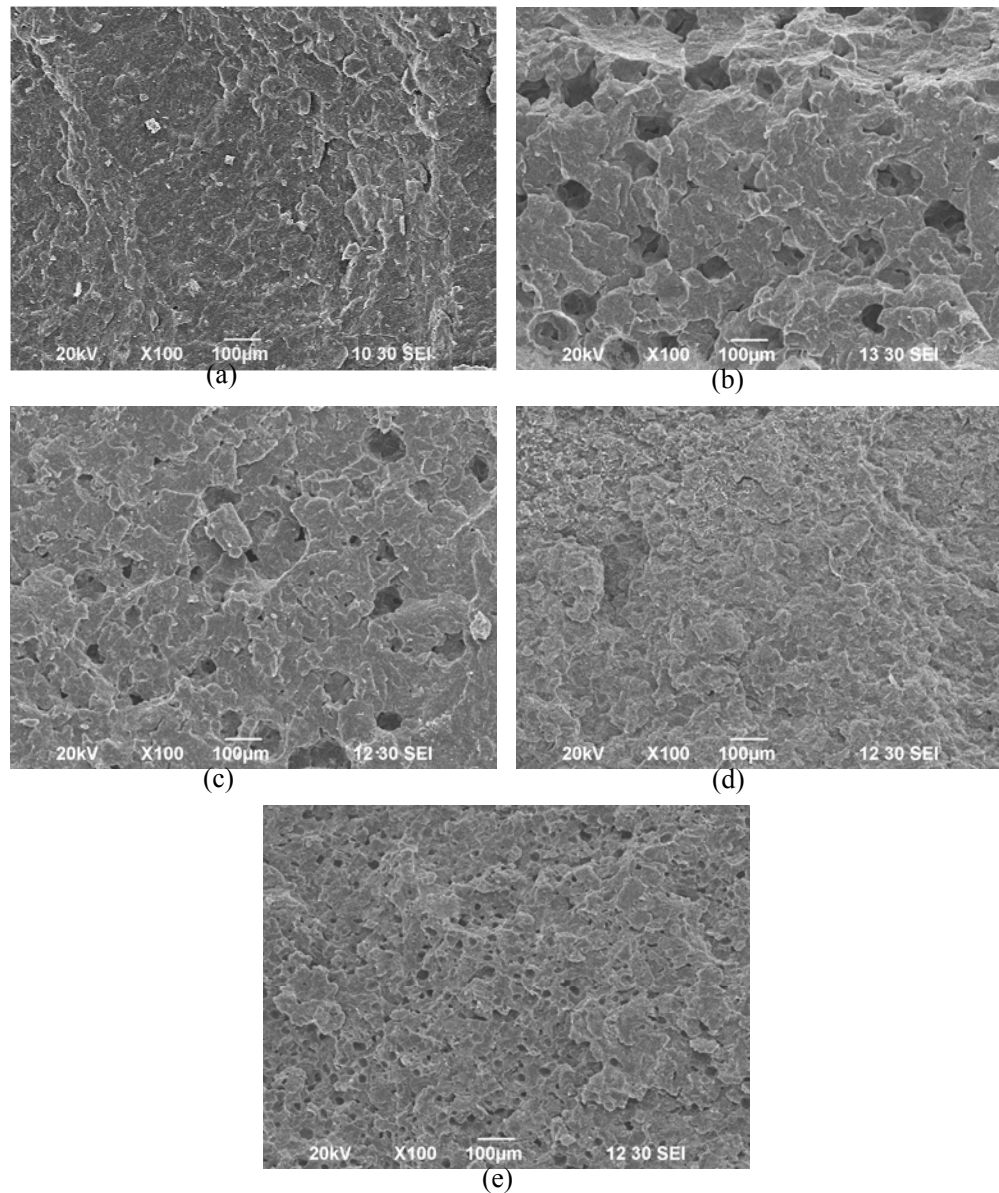
Fig.3.10 SEI-SEM micrographs of the fracture surfaces: (a) pure PP, and sintered PP/CNT/HA composites (b) 100:1:0, (c) 100:1:5, (d) 100:1:15 and (e) 100:1:30

In Fig.3.10, it can be observed that pores were generated in all the sintered PP/CNT/HA samples. By comparing the porosity of the PP plate and the microwave sintered composites, the porosity firstly increases from the PP plate in Fig.3.10(a) to a peak at 100:1:0, as shown in Fig.3.10(b), then decreases all the way from the peak to a valley at 100:1:15, as shown in Fig.3.10(d), and finally increases from the valley to 100:1:30 in Fig.3.10(e). In summary, the porosity of the unmodified PP and sintered composites shows an *S*-shaped trend with an increase in HA content, and the lowest porosity occurs at 100:1:15.

A similar *S*-shaped porosity trend was reported for some other multi-particle systems in conventional sintering (Dessieux *et al.*, 1976; Savitskii *et al.*, 2000). Savitskii *et al.* introduced a multi-particle model to explain the trend for a two component sintering system (Savitskii, 2009). In their model, it was assumed that the predominant atom flow was from a component *A* to another component *B* during conventional sintering. Firstly, the porosity for pure *B* is low, then at a low *A* concentration, each *A* particle was surrounded by a circle of *B* particles. During sintering, *B* expanded after receiving atoms from *A* and generated an arch effect, inducing stresses in the compact and resulting in an entire volume increase. As the mixture concentration changed to a condition that each *B* particle was surrounded by *A* particles, the *A* particles were absorbed by *B* particles, thus resulting in densification.

In the current study, for composites with ratios 100:1:0 and 100:1:5 in which the filler content is low, PP particles may diffuse and combine with each other after absorbing the energy from microwave irradiation. During the diffusion process, stresses may be

induced and thus the entire volume expands. As the HA content increases to a condition that the surrounding PP particle for 100:1:15, as shown in Fig.3.7(c), HA and MWCNT fillers may bond and combine with PP particles at the sintering temperature. When the HA content further increases to 100:1:30, the diffusion rate increases with higher energy absorption. Therefore more pores can be observed in the sintered sample, as shown in Fig.3.10(e).

3.2.4 PP Matrix Crystallization and Melting Characterization

As reviewed in the previous chapter, the nucleating effect of the PP matrix could be affected by introducing CNTs, which may further influence the mechanical properties of the resulting materials. In this section, the crystallization and melting behaviour are studied for the fabricated composites.

Differential scanning calorimetry (DSC, Perkin Elmer DSC-7) was adopted to characterize the crystallization and melting properties of the PP matrix of the microwave sintered composites. The as-received PP powder was used as control. Each sample of about 8 mg was heated from 30 to 200 $^{\circ}$C at 10 $^{\circ}$C min^{-1}. In order to eliminate the thermal history, the sample was then held at 200 $^{\circ}$C for 5 min. Finally, the sample was cooled and re-heated at the same rate. Thermal analysis was conducted by using the first cooling and the second heating.
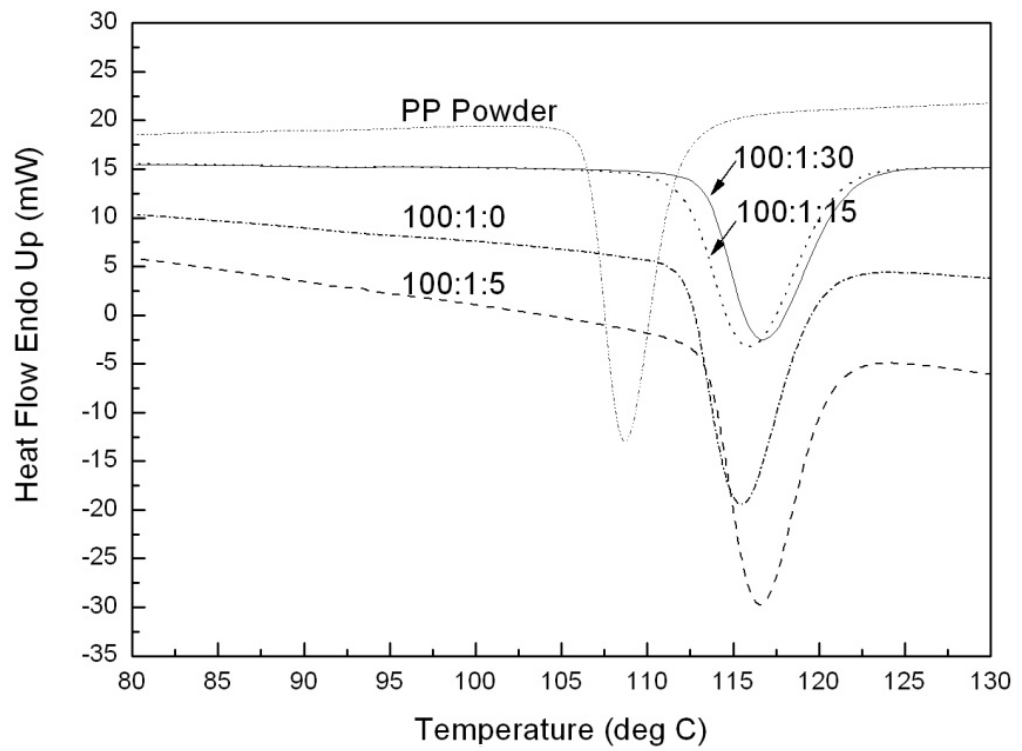
(a)
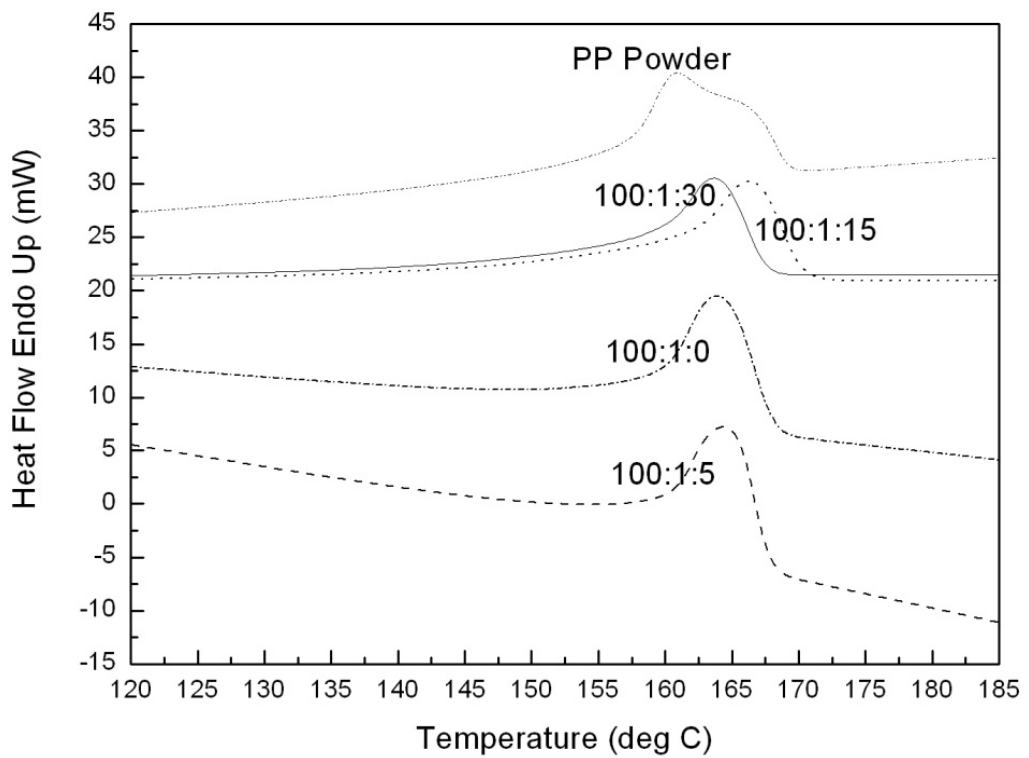
(b)

Fig.3.11 DSC thermograms of melting and crystallization of the composites: (a) crystallization and (b) melting

Table 3.2 is a summary of the thermal properties including the crystallization temperature (T_c), crystallization enthalpy (H_c), melting temperature (T_m), melting enthalpy (H_m) and the degree of crystallinity (H^*). H^* denotes the PP crystallinity in the PP/CNT/HA composites, which was obtained using Equation (3-1).

$$H^* = H_c/(1 - \varphi)\Delta H_m \qquad\qquad (3\text{-}1)$$

where ΔH_m is the heat fusion of isotactic PP with 100% crystallinity (209 J/g) (Martuscelli *et al.*, 1982; Xu *et al.*, 2008), and φ is the PP weight fraction in the PP/CNT/HA composites. The H_c values were obtained by calculating each area of the crystallization peaks in Fig.3.11 (a).

Table 3.2 Thermal properties of the PP/HA/CNT composites

Sample	T_c ($^{\circ}$C)	H_c (J g^{-1})	T_m ($^{\circ}$C)	H_m	H^*(%)
PP powder	108.63	-124.25	160.87	108.27	59.45%
100:1:0	115.47	-126.60	163.87	116.45	61.18%
100:1:5	116.47	-126.25	164.53	123.82	64.03%
100:1:15	115.97	-112.37	166.20	102.56	62.37%
100:1:30	116.24	-98.59	163.70	90.25	61.80%

As shown in Table 3.2, for all composites, T_c, T_m and H^* are higher than those of the as-received PP, suggesting the nucleating enhancing effect of the CNT and HA fillers. A similar nucleating effect was observed for CNT (Valentini *et al.*, 2003) and HA (Liu *et al.*, 2007) composites.

The H^* value first increases with addition of the HA content from a low point at the PP powder to the peak at a composition of 100:1:5, and then decreases with further increment of HA content until a ratio of 100:1:30 is reached. Similar crystallinity degree peaks at mid HA content was also observed for PLLA/HA composites (Hong *et al.*, 2005). The credibility of the H^* decrement at high filler content may be seen by the analysis in which the presence of a large amount of filler may somewhat hinder the ability of PP chains to incorporate into crystalline lamella, generating a number of defects and less ordered polymer crystals (Wu *et al.*, 2008a).

For H_c and H_m, the increments at low filler content (100:1:0 and 100:1:5) as compared with raw PP suggest the enhancement of crystallinity by introducing the CNT and HA particles, while the following descending trend at higher filler content (100:1:15 and 100:1:30) may be due to the relatively smaller amounts of PP in the composites.

3.2.5 Dynamic Mechanical Analysis

Dynamic mechanical analysis (DMA, Perkin Elmer Diamond DMA Lab System) was conducted in a nitrogen atmosphere in the tensile mode, with an oscillation amplitude of 10 μm at three fixed frequencies of 0.1, 1 and 10 Hz. The samples in the test were of rectangular shape 18, 3 and 1 mm in length, width and thickness, respectively. The temperature was swept from 30 to 180 ^{o}C at a rate of 3 ^{o}C/min. The storage modulus (E'), loss modulus (E'') and loss tangent ($Tan\delta$) were recorded. Figs.3.12(a) and (b) show the DMA thermograms at 1Hz for different compositions, as well as at different frequencies for 100:30:1, respectively.
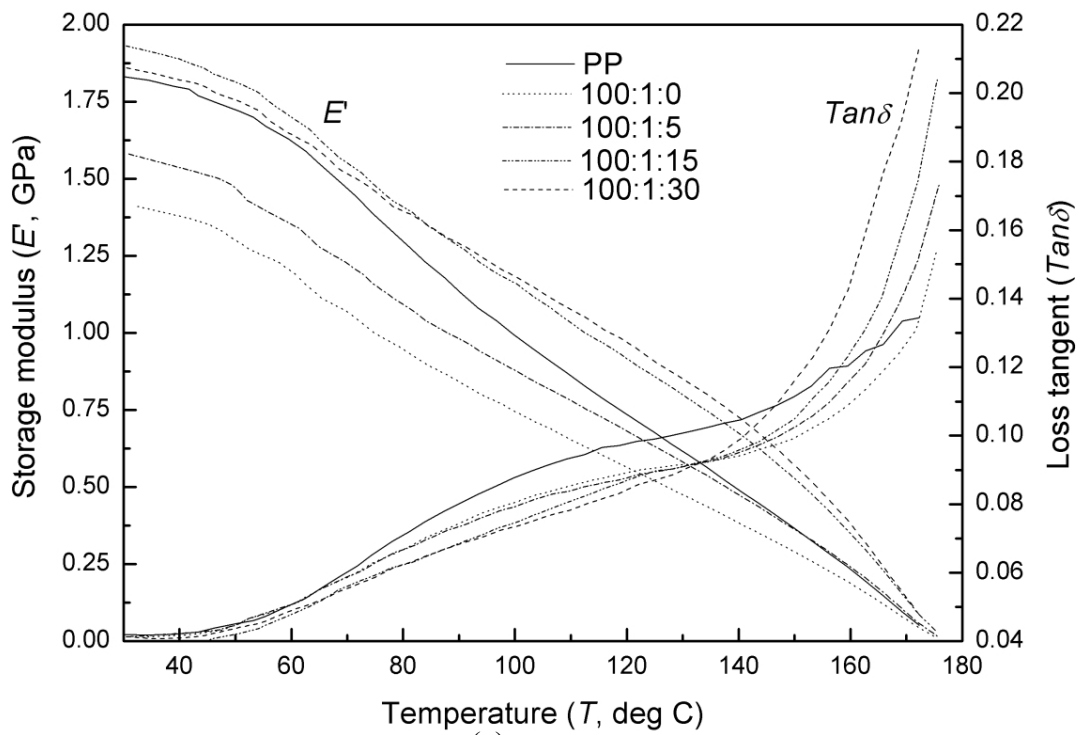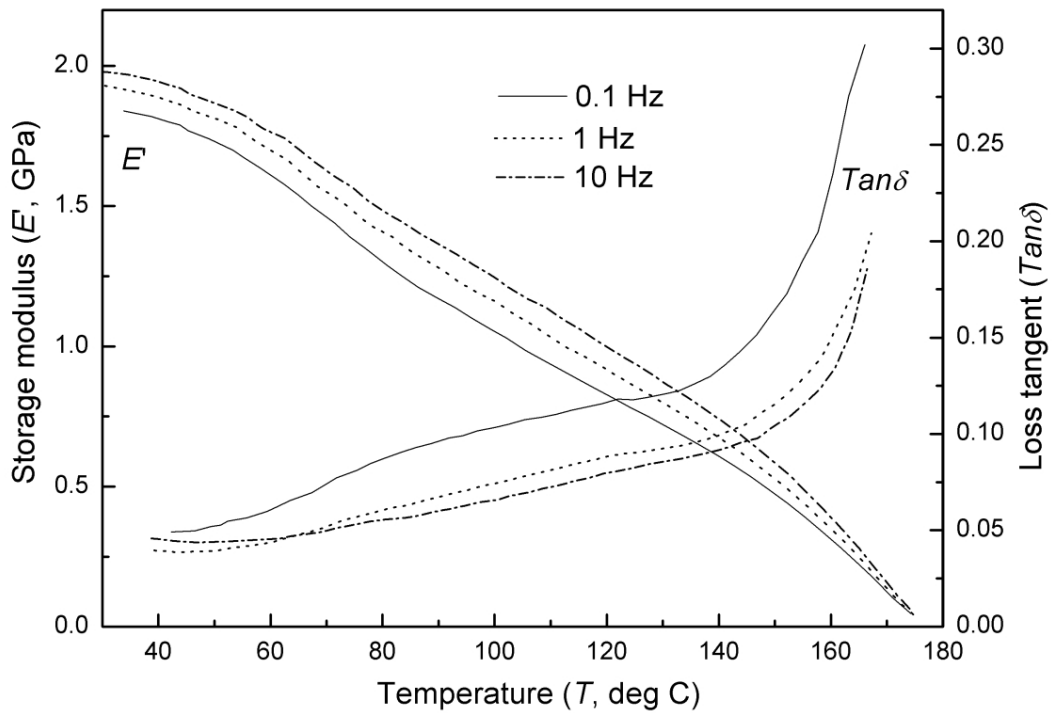
Fig.3.11 DMA thermograms of the storage modulus (E') and loss tangent ($Tan\delta$) versus temperature (T) curves for (a) at 1 Hz for different composite compositions, and (b) at different frequencies for a composition of 100:1:15

Nano-HA may act as a reinforcing agent. It can be seen from Fig.3.12(a) that the 100:1:15 and 100:1:30 composites showed a slight increase in the storage modulus. A similar reinforcing effect was reported for some similar bioceramic-polymer composites (Liu *et al.*, 2007; Wang *et al.*, 1997). However, it should be noted that the storage modulus *E'* of pure PP is higher than that of 100:1:0 and 100:1:5 in the complete measured temperature range. This may due to the poor bonding between the PP and nano-HA at low content or the effect of porosity.

Further study on the reinforcing effect of the HA yielded interesting results. As shown in Fig.3.12(a), the composite 100:1:30 shows a lower E' value as compared with the 100:1:15 at low temperature (30-80 ^{o}C), which may due to the effect of the porosity within the composite 100:1:30, as shown in Fig.3.10(e). However, it is the opposite when temperature goes higher than 90 ^{o}C, which is similar to a previously reported phenomenon that the HA reinforcing effect in the storage modulus beyond T_g is greater than that below T_g (Chen *et al.*, 2007).

In addition to the reinforcing effect, another important result is the loss tangent *Tanδ*. The *Tanδ* is the ratio of the dissipated energy to the stored energy per cycle, i.e., E''/E'. The lower the value, the higher the dimensional stability. In Fig.3.12(a), the introduction of HA reduces the loss tangent as compared with pure PP in the temperature range from 30 ^{o}C to 130 ^{o}C. A low *Tanδ* value in this temperature range means a high dimensional stability. Therefore, the *Tanδ* value suggests material favourability for hard tissue implant applications, such as in intervertebral disc

replacement where high dimensional stability under cyclic loads of about 2 million strides per year is required (Black *et al.*, 1998).

Finally, the effect of varying frequency on the dynamic mechanical performance of the composites was studied. Fig.3.11(b) shows this effect on the E' and *Tanδ* for the 100:1:15 composite. It indicates that more elastic-like behaviour in terms of lower *Tanδ* and higher E' values is induced under higher frequency. Comparable observations were also observed for similar composites (Chen *et al.*, 2007; Geethamma *et al.*, 2005).

Chapter 4: Elastic Modulus Evaluation of PP/CNT/HA Composites using Inverse Finite Element Method

4.1 Introduction

In this study, the fabricated samples were about 20 mm in diameter and around 3 mm in thickness, which were too small to follow standard mechanical tests. As a matter of fact, the mechanical evaluation techniques for small size specimens have attracted great research interest (Hyde *et al.*, 2007; Lucas *et al.*, 2002). The development of these techniques are greatly driven by the need in some cases that the specimens are too small for the standard tests, which are especially preferred where large specimens may put the components at risk (Hyde *et al.*, 2007). In addition to the case where standard size specimens are not available, the development of the research on functionally graded materials, such as biomedical graded materials (Pompe *et al.*, 2003), requires the characterization of the material non-homogeneity, for which small size specimen testing techniques are also of great importance (Kurtz *et al.*, 1997; Tang *et al.*, 2003). Among all small size specimen techniques, one of the most commonly adopted is the small punch testing technique.

The small punch testing technique was firstly used for mechanical characterization of metals (Foulds *et al.*, 1995; Mao *et al.*, 1991). More recently, application of this technique has been extended to the mechanical properties evaluation of polymeric materials. It has been adopted to evaluate the elastic modulus (Kurtz *et al.*, 1997), and qualitatively evaluate some other mechanical properties, such as wear properties and

toughness (Akagi *et al.*, 2006; Kurtz *et al.*, 1999; Tang *et al.*, 2003). This technique has been found to be reproducible and effective for the elastic behaviour characterization of PMMA (Giddings *et al.*, 2001), and could be readily adopted to evaluate the mechanical properties of the PE components for total joint arthroplasty (Kurtz *et al.*, 1999).

The elastic modulus prediction by this small punch testing technique can be achieved by three steps (Kurtz *et al.*, 1997). Firstly, initial stiffness of a material is measured from a load-displacement curve from a punch process. Secondly, an inverse finite element (FE) model for the punch process is constructed to obtain a correlation of initial stiffness and elastic modulus for the material. Finally, the elastic modulus of the material can be determined from the measured initial stiffness by using the predicted correlation.

While success has been achieved to some extent, some problems exist in this small punch testing technique due to the limitation of the device design. A typical design consists of a testing guide and die, a hemispherical head punch, and a disc-shaped specimen which is supported by a ring support and indented by the hemispherical punch (Kurtz *et al.*, 1997). In this ring support based design, it is entirely possible that not all parts of the ring support fully contact the specimen during the punch process, either due to operation variation or specimen dimensional error, which may further influence the accuracy of the experimental results. Another potential disadvantage may arise from the large contact surface area between the specimen and the ring support. This may result in a relatively large slope for the linear curve of initial stiffness versus elastic modulus within the elastic range, i.e., low sensitivity for elastic modulus prediction for a certain

initial stiffness, which is not preferred in the measurement.

The finite element approach has been widely used to analyze the mechanical response of various materials (Mijuca, 2008; Tang *et al.*, 2007), and is useful for the determination of material properties which may be difficult to be obtained by purely experimental methods (Bala *et al.*, 2006). In this part of study, a finite element based small punch testing method was developed to determine the elastic modulus of small specimens.

Sections 4.2 and 4.3 describe an attempt to develop and validate the small punch testing method, by using three different kinds of small polymeric specimens: PE, PP and PMMA. After validation, the developed method was then used to evaluate the elastic modulus of the fabricated microwave sintered specimens in section 4.4.

4.2 Development of the Finite Element Based Small Punch Testing Method

4.2.1 Finite Element Models of the Punch Process

A three-dimensional FE model was constructed by ABAQUS/Standard (Hibbit, Karlsson & Sorensen, Inc, Pawtucket, RI) to simulate a punch process using a small three-point support based testing device, and to predict the correlation of initial stiffness and elastic modulus of small polymer specimens. In this model, the support and punch were represented by rigid surfaces, while a disc-shaped specimen of 20.0 mm in diameter and 2.5 mm in thickness was considered as a deformable part constructed from

32,726 hex-dominated elements. The diameter of the circle passing through the three spherical centres of the three-point support was 7.9 mm. The diameters of hemispherical heads of both the support and punch were 3.9 mm. The areas of the deformable specimen that may contact the rigid surfaces were meshed, with refinement as shown in Fig.4.1.
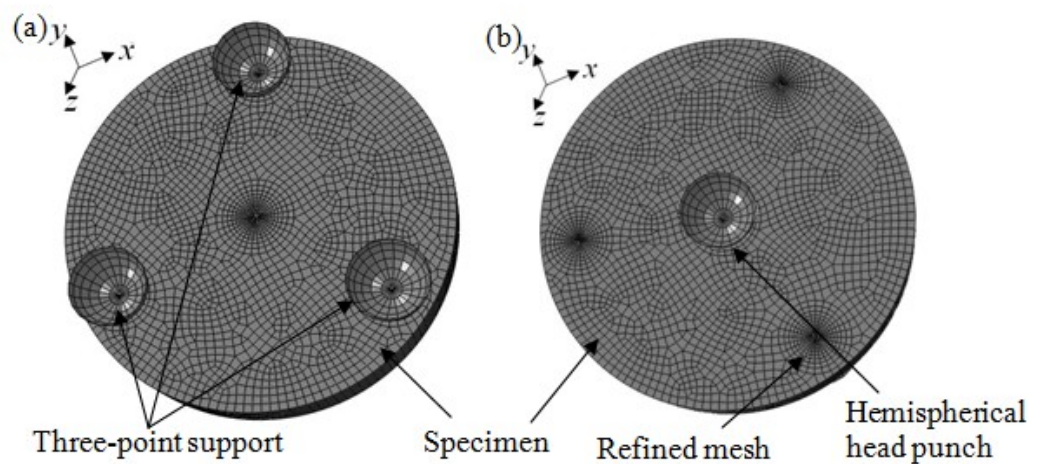
Fig.4.1 Finite element mesh of the three-point support based small punch testing device and specimen, (a) lower view and (b) upper view

The contact pairs of the punch-specimen and support-specimen were simulated using the penalty stiffness method (Kurtz et al., 1997), so as to allow some relative motion between the surfaces. During simulation, a small punch displacement of 0.01 mm was introduced before the punch process to build a firm contact between the specimen and the hemispherical heads. The circular plane of the specimen was positioned parallel to the x-y plane, while the thickness direction of the specimen was along the z axis. The support was constrained along all the x, y and z directions, while the punch was fixed along the x and y directions. The circumference of the specimen was constrained in all

directions including both translation and rotation before the firm contact was built, after which all the constraints were removed. A friction coefficient of 0.05 between the contact surfaces was adopted from similar work (Kurtz *et al.*, 2002). Poisson's ratios (v) of 0.46~0.47 for the PE obtained from a material datasheet from Goodfellow[TM] and a further reference (van Krevelen *et al.*, 2009) were adopted, while those of PP (0.42~0.45) were acquired from the material datasheet from INEOS Olefins & Polymers USATM and another reference (Lo *et al.*, 2005). The values of v for PMMA were set to 0.35~0.40 with reference to the material datasheet from Goodfellow[TM].

Table 4.1 Definition of the variables used in the present work

Variable	Designation (unit)
Prescribed punch displacement	D_p (mm)
Measured punch force	F_m (N)
Measured initial stiffness of the specimen	k_m (N/mm)
Computed punch force	F_s (N)
Computed initial stiffness of the specimen	k_s (N/mm)
Parametrically given elastic modulus of the specimen	E_p (MPa)
Elastic modulus of the specimen determined from the developed method	E_m (MPa)
Elastic modulus of the specimen determined from the bulk test	E'_m (MPa)

From the simulation, a load-displacement curve was constructed using the prescribed

punch displacement (D_p) of 0.05 mm, and the corresponding computed punch force (F_s).

The parametrically given elastic modulus of the specimen (E_p) was varied within a range from 600 to 3000 MPa in steps of 200 MPa for each simulation, from which a corresponding computed initial stiffness of the specimen (k_s) was obtained by linearly fitting the curve of F_s versus D_p within a certain range of D_p. After a number of these simulations with varying E_p, the correlation of k_s versus E_p was found. By substituting k_s with k_m from the experimental curve, the corresponding elastic modulus (E_m) could be determined. The variables used in the present work are presented in Table 4.1.

4.2.2 Experimental Details

To measure the initial stiffness of the specimens, k_m, a novel three-point support based small punch testing device in connection with the tensile tester (Instron 3344), as shown in Fig.4.2, was designed and produced for undertaking the punch process.
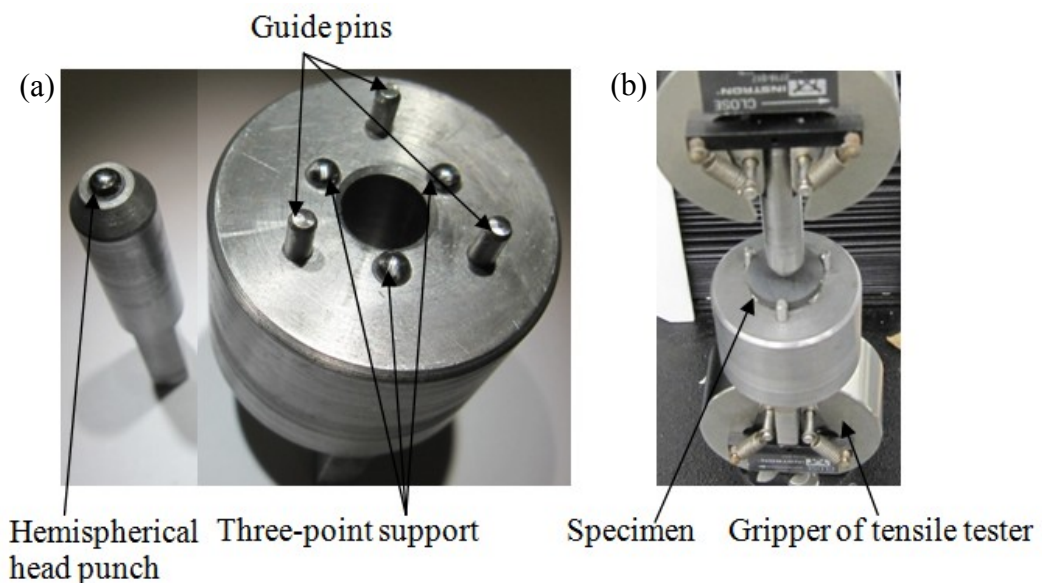
Fig.4.2 Three-point support based small punch testing device: (a) punch and support (b) with connection to the tensile tester

For the developed device, the coordinates of the spherical centres of the hemispherical heads of the three-point support and the punch, and the positions of the guide pins were determined with the aid of a high performance video measurement system (SmartScope Flash 300). The dimensions of the support, punch and specimens were the same as those used in the finite element study. The circle tangent to the inner surface of the three guide pins was 20.1 mm in diameter, which indicated the suitability of the pins for fixing a specimen 20 mm in diameter. The guide pins here are used just for determining the position of the specimen, not for fixation. These dimensions, together with a chamfer, were designed to ensure that the upper and lower surfaces of the specimen could not contact any part of the device other than the support and the punch head, during the punch process.

In this study, five disc-shaped specimens for each of the PE, PP and PMMA polymers were tested by using the developed testing device. The specimen was put on the three-point support, and then loaded with the hemispherical head punch at a constant displacement rate of 0.5 mm/min, which was based on other similar work (Kurtz et $al.$, 1997). During the experiment, a curve of measured punch force (F_m) versus punch displacement (D_p) was digitally recorded. Initial tests showed that the linear (elastic) portion of the load-displacement curve occurred at a displacement of less than 0.05 mm. The measured initial stiffness of the specimen (k_m) was calculated by analyzing the curve up to the displacement of 0.05 mm. Each set of specimens was tested six times at each 60º location around the specimen central point. The curve for each test was analyzed by linear fitting. The relative experimental uncertainty was calculated with reference to similar work, i.e., dividing the standard deviation by the average value for

each of the three material groups (Kurtz *et al.*, 2002).

As controlled experiments, tensile tests, designated as "bulk tests" below, were conducted for measurements of elastic moduli (E'_m) of the PE, PP and PMMA specimens by following the requirements of the ASTM D 638-08 Standard using tensile bars with type IV dimensions. The results obtained from the finite element based method and the bulk tests were analyzed by *t*-tests, and a *p*-value of 0.05 was used for testing the statistical significance of their differences.

4.3 Validation of the Small Punch Testing Method

4.3.1 Determination for Elastic Moduli of PE, PP and PMMA

By using the finite element based method, the loading process of the small punch test was simulated for determining the correlation of the elastic modulus, E_p and the initial stiffness, k_s of three small PE, PP and PMMA specimens. Contours of the von Mises stress at a punch displacement of 0.05 mm for the specimen with a Poisson's ratio of 0.35 and elastic modulus of 3000 MPa are shown in Fig.4.3.

In Fig.4.4, the curves ($r^2 > 0.99$) of F_s versus D_p for specimens with a fixed Poisson's ratio (v=0.35) and with varying E_p increases from 600 to 3000 MPa in steps of 200 MPa are presented. Fig.4.3 and Fig.4.4 indicate that the specimens exhibit elastic responses for the punch displacement within the 0.05 mm range.
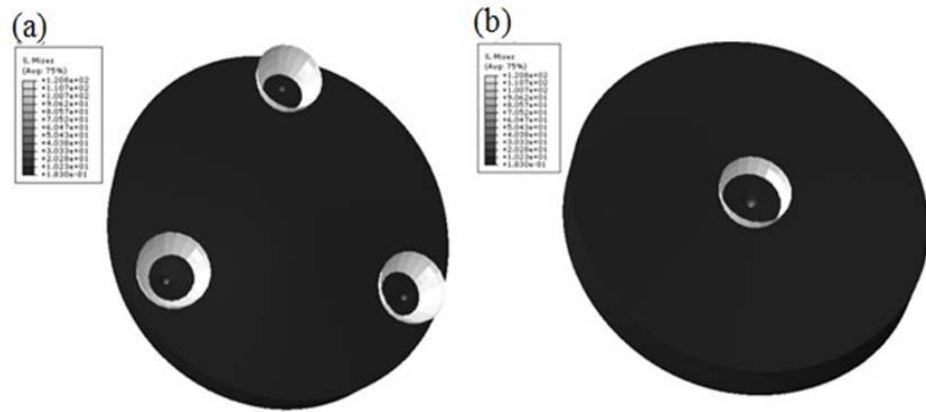
Fig.4.3 Contours of von Mises stress at a punch displacement (D_p) of 0.05 mm for the specimen with a Poisson's ratio (v=0.35) and elastic modulus (E=3000 MPa): (a) lower view and (b) upper view
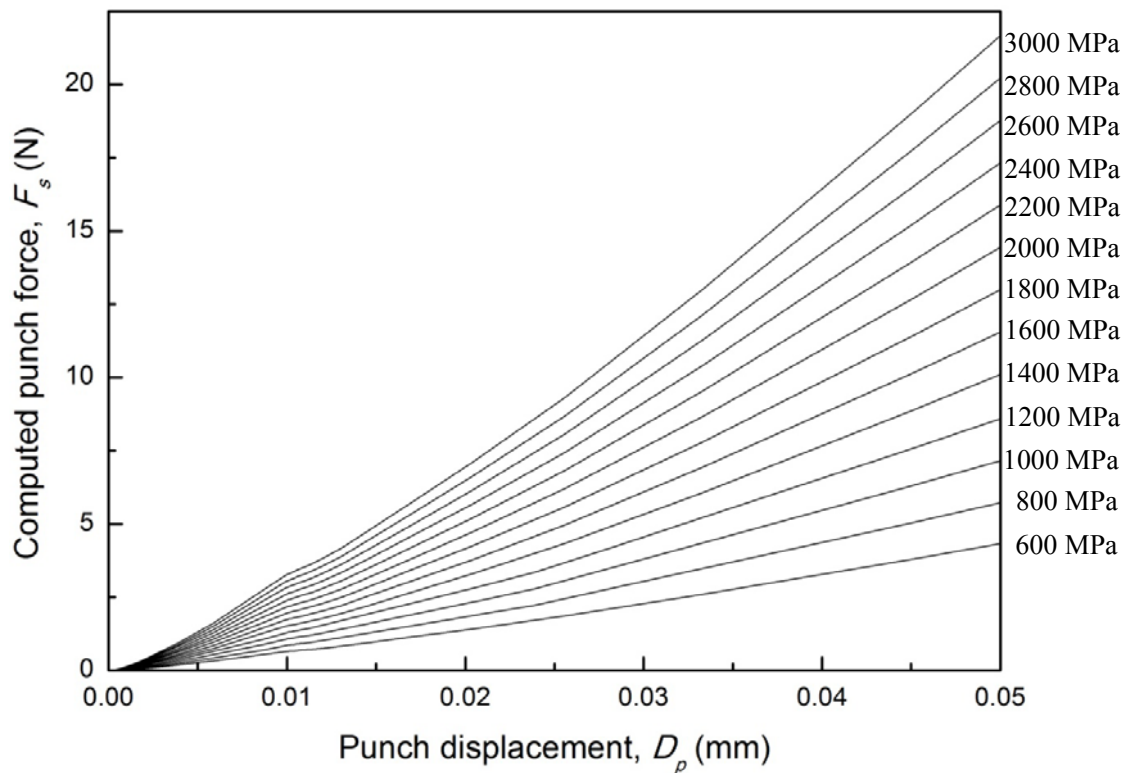
Fig.4.4 Computed punch force (F_s) versus punch displacement (D_p) for specimens with Poisson's ratio (v=0.35) and parametrically given elastic modulus (E_p=600-3000 MPa)

Since a punch displacement of 0.01 mm was introduced to enable a firm contact during the FE analysis, a short range of non-linearity can be observed at the punch displacement of 0.01 mm in each curve in Fig.4.4. Therefore, a punch displacement range from 0.02 to 0.05 mm was used to determine the computed initial stiffness of the specimen, k_s. For each studied polymer, k_s could be linearly correlated with E_p for each Poisson's ratio, v. The linear correlations between k_s and E_p of PE ($v = 0.46\text{-}0.47$), PP ($v = 0.42\text{-}0.45$) and PMMA ($v = 0.35\text{-}0.4$) ($r^2 > 0.9$) are expressed by the following equations (4-1)~(4-3), respectively.

$$k_s = 0.1812{\sim}0.1845E_p \qquad\qquad (4\text{-}1)$$

$$k_s = 0.1757{\sim}0.1805E_p \qquad\qquad (4\text{-}2)$$

$$k_s = 0.1629{\sim}0.1709E_p \qquad\qquad (4\text{-}3)$$

After substituting k_s with k_m, and E_p with E_m in equations (4-1)~(4-3), the correlation between E_m and k_m, for PE, PP and PMMA can be expressed in the following equations (4-4)~(4-6), respectively.

$$E_m = 5.42{\sim}5.52k_m \qquad\qquad (4\text{-}4)$$

$$E_m = 5.54 \sim 5.69 k_m \qquad\qquad\qquad\qquad\qquad (4\text{-}5)$$

$$E_m = 5.85 \sim 6.14 k_m \qquad\qquad\qquad\qquad\qquad (4\text{-}6)$$

In order to evaluate the elastic moduli of the PE, PP and PMMA specimens, initial stiffness, k_m was measured by using the curves of F_m versus D_p as shown in Fig.4.5, which were obtained from the specially designed three-point support based small punch testing device. Due to the probability that the contact condition is not stable at the beginning, the initial stiffness for each specimen was calculated from a displacement between 0.02 and 0.05 mm. The curves within this displacement range were found to have a linear fit ($r^2 > 0.99$) for all specimens. The values of k_m for PE, PP and PMMA calculated within this displacement range were 145.2±4.9 N/mm, 234.4±4.6 N/mm, and 434.6±1.8 N/mm, respectively. The experimental uncertainties of k_m for all the tests were 2.9 % for PE, 1.8 % for PP and 0.4 % for PMMA. By using Eqs.(4-4)~(4-6), the elastic moduli, E_m for PE, PP and PMMA were found to be 787±27~802±27 MPa, 1299±25~1334±25 MPa, and 2542±16~2668±16 MPa, respectively. The elastic moduli obtained from the bulk tests, E_m', were 760±31 MPa for PE, 1245±29 MPa for PP and 2595±18 MPa for PMMA.
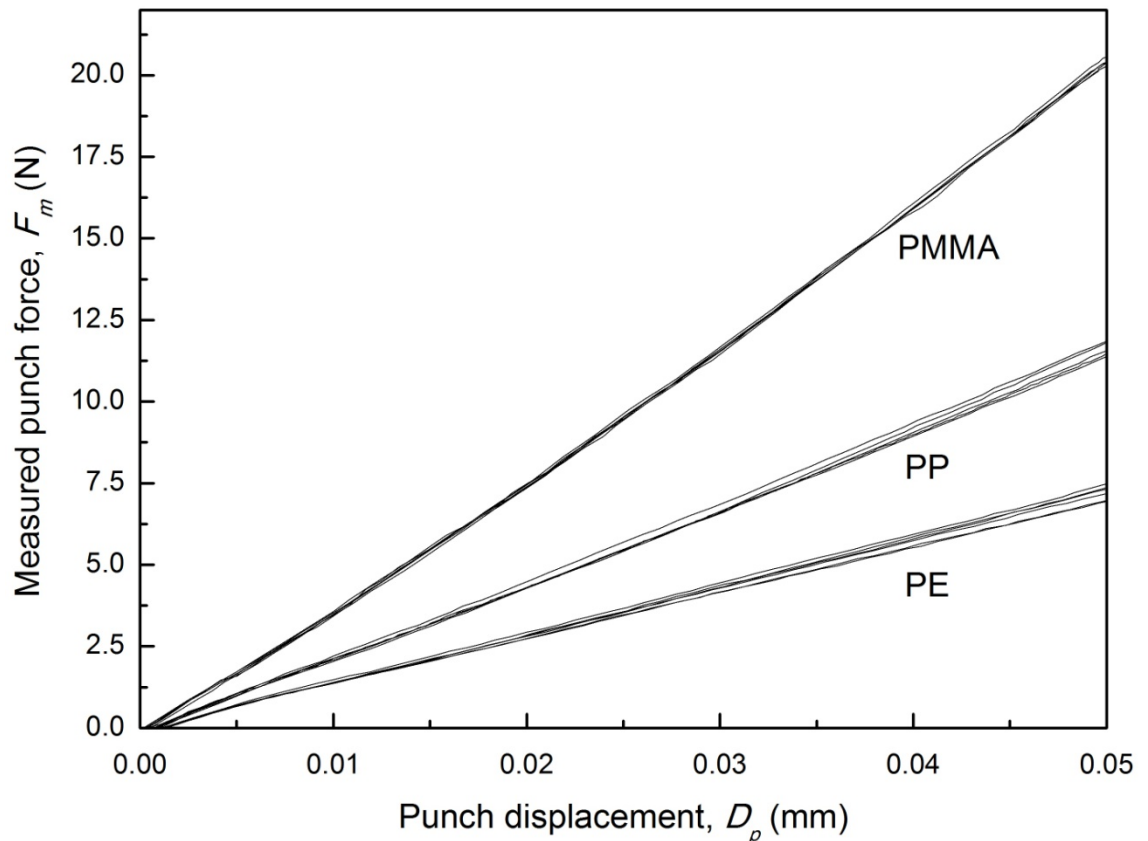
Fig.4.5 Measured punch force (F_m) versus punch displacement (D_p) curves from the three-point support based small punch testing technique for each typical specimen of PE, PP and PMMA

Fig.4.6 shows the curves of k_m versus E_m for PE, PP and PMMA specimens with the corresponding v range obtained by using the developed finite element based method and the bulk tests. PMMA is within the range of the elastic values predicted for v=0.35~0.40. No statistical significance ($p > 0.05$) for the difference in the elastic moduli, E_m, of PE, PP and PMMA was observed for v=0.46~0.47, v=0.45 and v=0.40, respectively, as compared with the bulk testing results, E'_m. Thus, the developed finite element based method was validated as an effective tool for determining the elastic moduli of polymers.
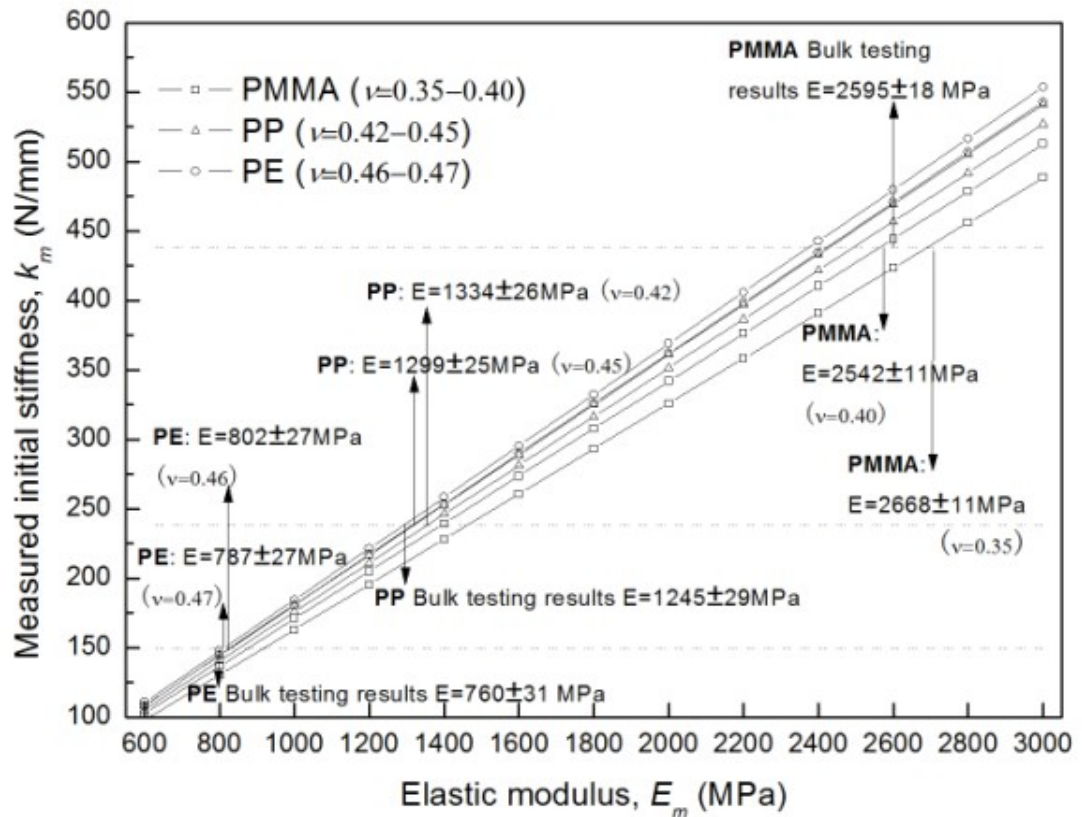
Fig.4.6 Measured initial stiffness (k_m) versus elastic modulus (E_m) for PE, PP and PMMA specimens with corresponding Poisson's ratio (v) range, determined by the developed method and bulk test

4.3.2 Accuracy and Sensitivity of the Small Punch Testing Method

In order to compare the developed finite element based method and the ring support type small punch testing method in terms of accuracy and sensitivity, another two separate FE models were constructed. The boundary conditions of the model described above were adopted here for these two series of simulations. During a real loading process, it is impossible to ensure that the punch is located at the centre of the specimen,

which may lead to certain errors. In each series of simulations, punch head eccentricities of 0.0, 0.2, 0.5, 1.0 and 2.0 mm were considered and simulated as potential errors. In the two series of simulations, the specimen dimensions, the inner diameters of both supports and the diameters of both punches were the same. The diameter of the circle passing through the three peaks of the three-point support was 7.5 mm, and the diameter of the each head of the support was 3.0 mm, i.e., the inner diameter of the three-point support was also 6.0 mm, the same as that for the ring support. The head diameters of the two punches were both 3.0 mm. The Poisson's ratios, v, for both series of simulations were chosen as 0.46.

In this subsection, the results of the comparison in terms of accuracy and sensitivity between the developed method and the ring support based small punch testing method are presented and discussed. When the punch force was applied at 2.0 mm eccentrically away from the specimen centre, the contours of the von Mises stress at the deformation $D_p = 0.05$ mm, are shown in Fig.4.7 for the three-point and the ring supporting cases. Fig.4.7 indicates that the material exhibits elastic behaviour at the 0.05 mm punch displacement. The maximum von Mises stress in Figs.4.7 (a) and (b) for the three-point support based small punch testing technique is lower than that in Figs.4.7 (c) and (d) for the ring support based one, suggesting the k_s value obtained from the three-point support based technique may be lower than that from the ring support method.
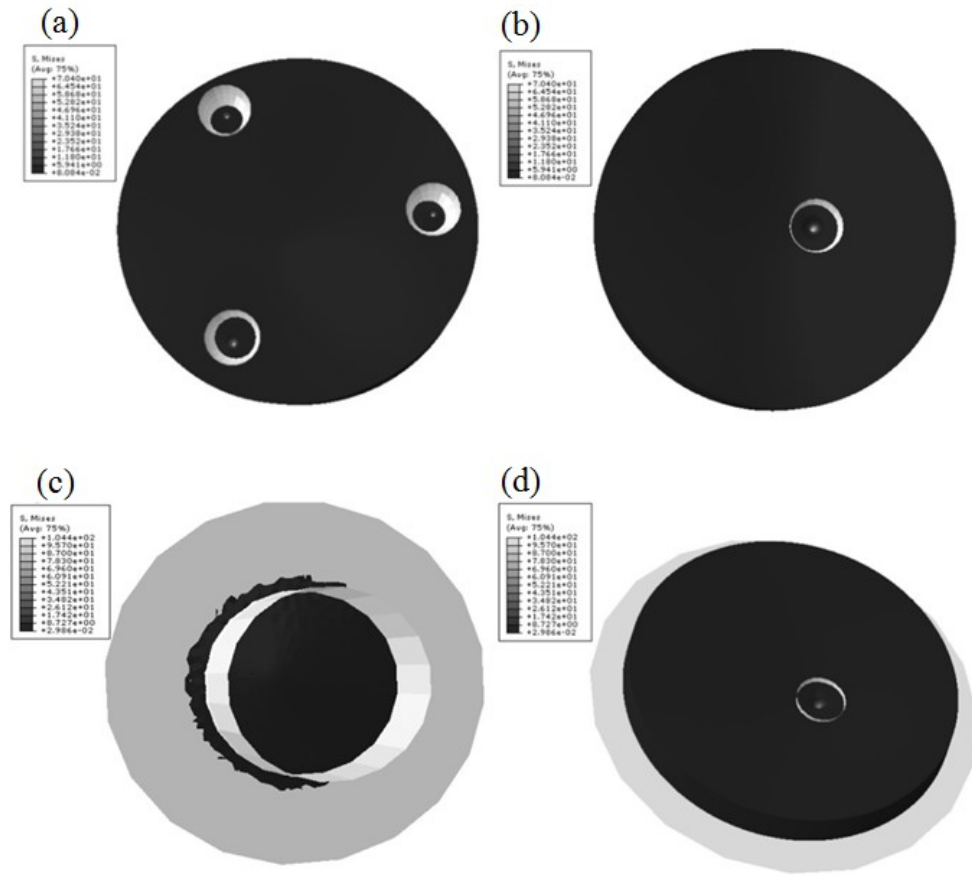
Fig.4.7 Contours of von Mises stress at a punch displacement (D_p) of 0.05 mm when the punch is 2.0 mm horizontally away from the specimen centre. The finite element based method: (a) lower view and (b) upper view; ring support based small punch testing method: (c) lower view and (d) upper view

The curves of k_s versus E_p are shown in Fig.4.8. It can be seen from Fig.4.8 that the slopes of the curves obtained by using the three-point type method are smaller than those from the ring support type. When replacing k_s with a certain value of k_m in Fig.4.8, the variation of the E_m value obtained from the proposed method in response to the variation of k_m value is more sensitive than that from the ring support one. In addition to the higher sensitivity, the measurement accuracy of the developed method is higher.

Actually, the error of k_s at a 2.0 mm eccentricity, as compared to no eccentricity, for the developed method is 1.8 %, while that for ring support type is 8.6 %. In terms of the sensitivity and accuracy, the developed method is better compared with the conventional ring support type.
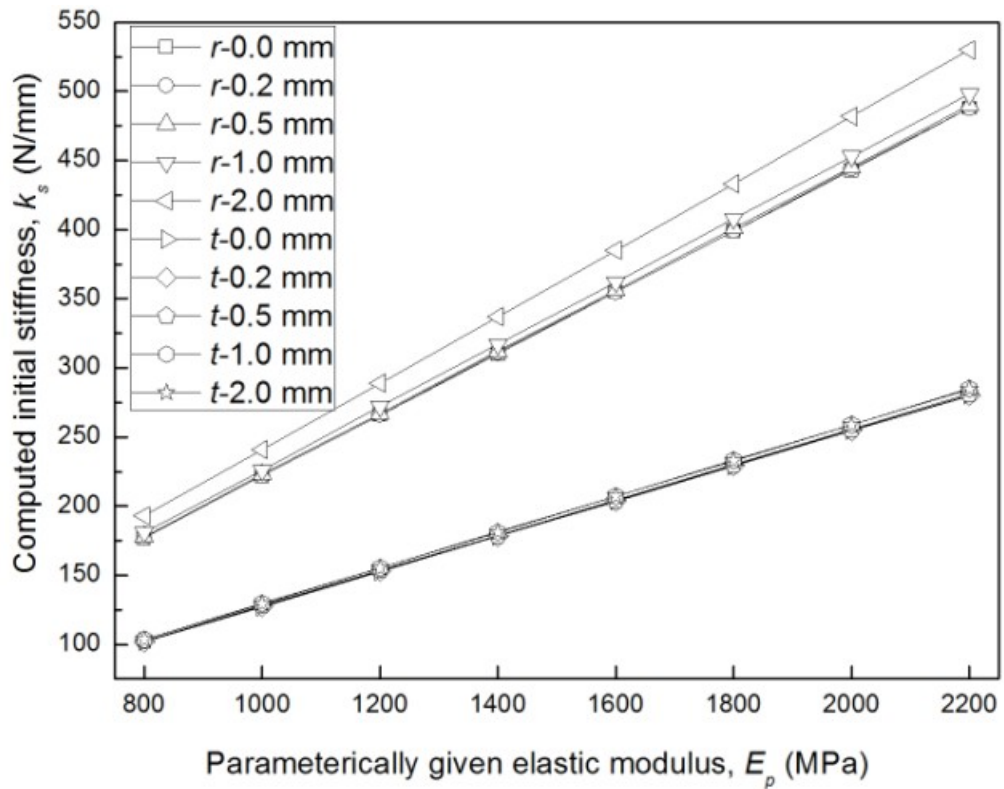
Fig.4.8 Computed initial stiffness (k_s) versus parametrically given elastic modulus (E_p) for the three-point support (designated as "t-") and the ring support type (designated as "r-") with punch eccentricities of 0.0, 0.2, 0.5, 1.0 and 2.0 mm from the centre

4.4 Elastic Modulus Evaluation the Fabricated PP/CNT/HA Composites

In this section, elastic moduli of the fabricated PP/CNT/HA composites were

determined. A combination of punching tests and FE simulation was adopted for the elastic modulus evaluation of the fabricated composites. Each disc-shaped specimen was tested by loading with the hemispherical head punch at a constant punch displacement rate, during which a curve of punch force versus punch displacement up to 0.05 mm was recorded, from which k_m can be obtained. Each set of specimens was tested six times at each 60° location around the specimen central point. This was conducted in order to reduce the errors caused by non-homogeneity. The reduction of the errors caused by non-homogeneity can ensure an improved accuracy of the elastic modulus prediction in terms of the whole bulk. The loading process was simulated by the FE model described in Section 4.1. The friction coefficient between the specimen and device was 0.05, and Poisson's ratio was 0.46. The specimen and device were simulated using their actual dimensions. The specimen was 20.0 mm in diameter and 2.5 mm in thickness. The diameter of the circle passing through the three spherical centres of the three-point support was 7.9 mm. The diameters of hemispherical heads of both support and punch were 3.9 mm. The elastic moduli are expressed by Equation (4-7).

$$E_m = 5.42 k_m \tag{4-7}$$

where the measured elastic modulus E_m is in MPa, and the measured stiffness k_m is in N mm^{-1}.

The elastic modulus E_m of the sintered PP/CNT/HA composites determined by the proposed technique is within the range 1.1 to 1.5 GPa, with acceptable deviation from

the control value of 1.22 GPa. It is suggested that the E_m value may be inversely influenced by the porosity, as shown in Fig.3.7. Further mechanical improvement may be achieved by improving the bonding between the filled particles and PP, and reducing the porosity.

Chapter 5: Overall Conclusions and Future Work

5.1 Overall Conclusions

In this study, microwave sintering of microwave transparent PP was made feasible by introducing CNT and HA fillers. Microwave sintering has the advantage of interacting directly with dielectric materials, thus reducing the processing time. Material characterization was conducted using microwave sintered composites, which evaluated the advantages and limitations of the proposed method. Moreover, a finite element based small punch testing method was developed to determine the elastic modulus of the composite specimens. To conclude, the main contributions of this study are summarized below:

(1) The PP/CNT/HA composites were successfully fabricated by microwave sintering. A reduction of the sintering time to less than 1 minute was achieved. Incorporation of CNT into the PP matrix can allow the microwave to interact directly with the composites to reduce the processing time. There was a significant reduction of sintering time as compared with the conventional polymeric material fabrication methods.

(2) The results of the material characterization tests show that the HA particles were uniformly distributed within the composites, suggesting the dispersion method with a combination of ultrasonication and mechanical stirring was effective. Filling of nano-HA up to 50 vol% in the composites could be achieved.

(3) A nucleating enhancement of the PP matrix with addition of HA and CNT fillers was revealed by the DSC characterization. The porosity variation showed an *S*-shaped trend versus compositions, among which the lowest porosity occurred at 100:1:15. DMA results showed a general increasing trend of storage modulus with HA addition, however, the porosity may have a strong influence on the storage modulus.

(4) A finite element based small punch testing method was developed for determining the elastic modulus of small polymeric specimens. In validation, this method was used to determine the elastic moduli of PE, PP and PMMA, which were found to have no statistical difference compared with those from standard tensile tests. Moreover, the sensitivity and accuracy of the developed method was confirmed to be higher than that of the conventional ring-support based small punch testing method. The method provides an alternative way for determining the elastic modulus for small polymeric specimens with high sensitivity and accuracy.

The findings of this project gave rise to the following research outputs:

1. *X. CHEN*, C.P. Tsui, C.Y. Tang. Finite element based small punch testing method for stiffness measurement of polymers, *Journal of the Serbian Society for Computational Mechanics*, in press.

2. *X. CHEN*, C.T. Wong, C.P. Tsui, C.Y. Tang. A feasibility study on microwave fabrication of PP/CNT composite, presented at *The Eighteenth Annual International Conference on Composites Engineering* (ICCE-18), July 2010, Anchorage, Alaska, USA.

5.2 Suggestions for Future Work

The outcomes of this project demonstrate the feasibility of microwave sintering to fabricate polymeric composites by using the PP matrix as an example. Further research may be conducted to investigate its application in fabricating similar composites composed of other polymer matrices as well as dielectric fillers. To better control the microwave power during sintering, a potential technique may be step heating. To better control the sintering process for composites with various compositions, a quantitative study should be conducted to examine the microwave field distribution and its interaction with corresponding materials. In this study, the reinforcing effect of the filled particles is not significant. It is, therefore, suggested to conduct certain chemical investigations on the surface modification of the filled particles for improving the strength of the interfacial bonding between the particles and the matrix. As PP based composites may be developed for implantation, biological tests are also suggested for further study.

References

Akagi, M., Asano, T., Clarke, I. C., Niiyama, N., Kyomoto, M., Nakamura, T., et al. (2006). Wear and toughness of crosslinked polyethylene for total knee replacements: A study using a simulator and small punch testing. *Journal of Orthopaedic Research, 24*(10), 2021-2027.

Anklekar, R., Agrawal, D., & Roy, R. (2001). Microwave sintering and mechanical properties of PM copper steel. *Powder Metallurgy, 44*(4), 355-362.

Armentano, I., Dottori, M., Puglia, D., & Kenny, J. (2008). Effects of carbon nanotubes (CNTs) on the processing and in-vitro degradation of poly (dl-lactide-co-glycolide)/CNT films. *Journal of Materials Science: Materials in Medicine, 19*(6), 2377-2387.

Assouline, E., Pohl, S., Fulchiron, R., Gerard, J., Lustiger, A., Wagner, H., et al. (2000). The kinetics of [alpha] and [beta] transcrystallization in fibre-reinforced polypropylene. *Polymer, 41*(21), 7843-7854.

Bala, I., Tang, C. Y., Tsui, C. P., Chen, D. Z., Uskokovi, P., Ignjatovi, N., et al. (2006). Nanoindentation of in situ polymers in hydroxyapatite/poly-L-lactide biocomposites. *Materials Science Forum, 518*, 501-506.

Baughman, R., Zakhidov, A., & De Heer, W. (2002). Carbon nanotubes--the route toward applications. *Science, 297*(5582), 787-792.

Behrend, M., Kluge, E., & Schuttler, W. (2006). On the use of unsealed polypropylene mesh as tracheal replacement. *ASAIO Journal, 52*(3), 328-333.

Bellón, J. M., Contreras, L. A., Buján, J., Palomares, D., & Martín, A. C.-S. (1998). Tissue response to polypropylene meshes used in the repair of abdominal wall defects. *Biomaterials, 19*(7-9), 669-675.

Best, S., Sim, B., Kayser, M., & Downes, S. (1997). The dependence of osteoblastic response on variations in the chemical composition and physical properties of hydroxyapatite. *Journal of Materials Science: Materials in Medicine, 8*(2), 97-103.

Bhattacharyya, A., Sreekumar, T., Liu, T., Kumar, S., Ericson, L., Hauge, R., et al. (2003). Crystallization and orientation studies in polypropylene/single wall carbon nanotube composite. *Polymer, 44*(8), 2373-2377.

Black, J., & Hastings, G. (1998). *Handbook of biomaterial properties*: Chapman & Hall.

Brosseau, C., Queffelec, P., & Talbot, P. (2001). Microwave characterization of filled polymers. *Journal of Applied Physics, 89*(8), 4532-4540.

Bykov, Y., Rybakov, K., & Semenov, V. (2001). High-temperature microwave processing of materials. *Journal of Physics D: Applied Physics, 34*(13), R55-R75.

Campanelli, G., Catena, F., & Ansaloni, L. (2008). Prosthetic abdominal wall hernia repair in emergency surgery: from polypropylene to biological meshes. *World Journal of Emergency Surgery, 3*(1), 33-36.

Cannon, R., & Carter, W. (1989). Interplay of sintering microstructures, driving forces, and mass transport mechanisms. *Journal of the American Ceramic Society, 72*(8), 1550-1555.

Chen, D. Z., Tang, C. Y., Chan, K. C., Tsui, C. P., Yu, P. H. F., Leung, M. C. P., et al. (2007). Dynamic mechanical properties and in vitro bioactivity of PHBHV/HA

nanocomposite. *Composites Science and Technology, 67*(7-8), 1617-1626.

Chen, Y., Gan, C., Zhang, T., Yu, G., Bai, P., & Kaplan, A. (2005). Laser-surface-alloyed carbon nanotubes reinforced hydroxyapatite composite coatings. *Applied Physics Letters, 86*(25), 251905.

Chen, Y., Zhang, Y., Zhang, T., Gan, C., Zheng, C., & Yu, G. (2006). Carbon nanotube reinforced hydroxyapatite composite coatings produced through laser surface alloying. *Carbon, 44*(1), 37-45.

Cheng, J., Agrawal, D., Komarneni, S., Mathis, M., & Roy, R. (1997). Microwave processing of WC-Co composities and ferroic titanates. *Materials Research Innovations, 1*(1), 44-52.

Chiang, W., & Wen-Der Yang, B. (1994). Polypropylene composites. III: Chemical modification of the interphase and its influence on the properties of PP/mica composites. *Polymer Engineering and Science, 34*(6), 485-492.

Chiu, W., Chang, Y., Kuo, H., Lin, M., & Wen, H. (2008). A study of carbon nanotubes/biodegradable plastic polylactic acid composites. *Journal of Applied Polymer Science, 108*(5), 3024-3030.

Cobb, W., Kercher, K., & Heniford, B. (2005). The argument for lightweight polypropylene mesh in hernia repair. *Surgical Innovation, 12*(1), 63-69.

Coleman, J. N., Khan, U., & Gun'ko, Y. K. (2006). Mechanical reinforcement of polymers using carbon nanotubes. *Advanced Materials, 18*(6), 689-706.

Cooper, C., Ravich, D., Lips, D., Mayer, J., & Wagner, H. (2002). Distribution and alignment of carbon nanotubes and nanofibrils in a polymer matrix. *Composites Science and Technology, 62*(7-8), 1105-1112.

Cosson, M., Debodinance, P., Boukerrou, M., Chauvet, M., Lobry, P., Crepin, G., et al.

(2003). Mechanical properties of synthetic implants used in the repair of prolapse and urinary incontinence in women: which is the ideal material? *International Urogynecology Journal, 14*(3), 169-178.

De Tayrac, R., Devoldere, G., Renaudie, J., Villard, P., Guilbaud, O., & Eglin, G. (2007). Prolapse repair by vaginal route using a new protected low-weight polypropylene mesh: 1-year functional and anatomical outcome in a prospective multicentre study. *International Urogynecology Journal, 18*(3), 251-256.

Denissen, H., Mangano, C., & Venini, G. (1985). *Hydroxylapatite implants*: Piccin Nuova Libraria.

Dessieux, R., Pozarnik, F., & Cizeron, G. (1976). Influence of particle size distribution on the importance of the Kirkendall effect occurring during powder mixture sintering. *Scripta Metallurgica, 10*(10), 865-870.

Downes, R., Vardy, S., Tanner, K., & Bonfield, W. (1991). Hydroxyapatite-polyethylene composite in orbital surgery. In W. Bonfield, G. W. Hastings, K. E. Tanner (Ed.), *Bioceramics, Vol.4*, (pp. 239-246): Butterworth Heinmann.

Drumright, R., Gruber, P., & Henton, D. (2000). Polylactic acid technology. *Advanced Materials, 12*(23), 1841-1846.

Duvall, J., Sellitti, C., Myers, C., Hiltner, A., & Baer, E. (1994). Effect of compatibilization on the properties of polypropylene/polyamide-66 (75/25 wt/wt) blends. *Journal of Applied Polymer Science, 52*(2), 195-206.

Esawi, A. M. K., Salem, H. G., Hussein, H. M., & Ramadan, A. R. (2010). Effect of processing technique on the dispersion of carbon nanotubes within polypropylene carbon nanotube-composites and its effect on their mechanical properties. *Polymer Composites, 31*(5), 772-780.

Fecek, C., Yao, D., Kacorri, A., Vasquez, A., Iqbal, S., Sheikh, H., et al. (2008). Chondrogenic derivatives of embryonic stem cells seeded into 3D polycaprolactone scaffolds generated cartilage tissue in vivo. *Tissue Engineering Part A, 14*(8), 1403-1413.

Feng, J., Sui, J., Cai, W., Wan, J., Chakoli, A., & Gao, Z. (2008). Preparation and characterization of magnetic multi-walled carbon nanotubes-poly (L-lactide) composite. *Materials Science and Engineering: B, 150*(3), 208-212.

Foulds, J., Woytowitz, P., Parnell, T., & Jewett, C. (1995). Fracture toughness by small punch testing. *Journal of testing and evaluation, 23*(1), 3-10.

Geethamma, V. G., Kalaprasad, G., Groeninckx, G., & Thomas, S. (2005). Dynamic mechanical behaviour of short coir fibre reinforced natural rubber composites. *Composites Part A: Applied Science and Manufacturing, 36*(11), 1499-1506.

German, R. (1989). *Particle packing characteristics*: Metal Powder Industries Federation.

German, R. (1996). *Sintering theory and practice*: Wiley.

Giddings, V. L., Kurtz, S. M., Jewett, C. W., Foulds, J. R., & Edidin, A. A. (2001). A small punch test technique for characterizing the elastic modulus and fracture behaviour of PMMA bone cement used in total joint replacement. *Biomaterials, 22*(13), 1875-1881.

Goldstein, A., Travitzky, N., Singurindy, A., & Kravchik, M. (1999). Direct microwave sintering of yttria-stabilized zirconia at 2·45 GHz. *Journal of the European Ceramic Society, 19*(12), 2067-2072.

Grimes, C. A., Mungle, C., Kouzoudis, D., Fang, S., & Eklund, P. C. (2000). The 500 MHz to 5.50 GHz complex permittivity spectra of single-wall carbon nanotube-

loaded polymer composites. *Chemical Physics Letters, 319*(5-6), 460-464.

Gross, K., Gross, V., & Berndt, C. (1998). Thermal analysis of amorphous phases in hydroxyapatite coatings. *Journal of the American Ceramic Society, 81*(1), 106-112.

Gupta, A., & Purwar, S. (1984). Crystallization of PP in PP/SEBS blends and its correlation with tensile properties. *Journal of Applied Polymer Science, 29*(5), 1595-1609.

Haggenmueller, R., Fischer, J., & Winey, K. (2006). Single wall carbon nanotube/polyethylene nanocomposites: nucleating and templating polyethylene crystallites. *Macromolecules, 39*(8), 2964-2971.

Haggenmueller, R., Gommans, H., Rinzler, A., Fischer, J., & Winey, K. (2000). Aligned single-wall carbon nanotubes in composites by melt processing methods. *Chemical Physics Letters, 330*(3-4), 219-225.

Harper, R., & Posner, A. (1966). *Measurement of non-crystalline calcium phosphate in bone mineral. Proceedings of the Society for Experimental Biology and Medicine, 122*(1), 137-142.

Harrison, B. S., & Atala, A. (2007). Carbon nanotube applications for tissue engineering. *Biomaterials, 28*(2), 344-353.

Hashin, Z., & Shtrikman, S. (1963). A variational approach to the theory of the elastic behaviour of multiphase materials. *Journal of the Mechanics and Physics of Solids, 11*(2), 127-140.

Hatzikiriakos, S., & Migler, K. (2005). *Polymer processing instabilities: control and understanding*: CRC.

Hench, L. (1998). Bioceramics. *Journal of the American Ceramic Society, 81*(7), 1705-

1728.

Hench, L., & Wilson, J. (1993). *An introduction to bioceramics*: World Scientific Pub Co Inc.

Hong, Z., Zhang, P., He, C., Qiu, X., Liu, A., Chen, L., et al. (2005). Nano-composite of poly(l-lactide) and surface grafted hydroxyapatite: Mechanical properties and biocompatibility. *Biomaterials, 26*(32), 6296-6304.

Hyde, T., Sun, W., & Williams, J. (2007). Requirements for and use of miniature test specimens to provide mechanical and creep properties of materials: a review. *International Materials Reviews, 52*(4), 213-255.

Iijima, S. (1991). Helical microtubules of graphitic carbon. *Nature, 354*(6348), 56-58.

Ikkala, O., Holsti-Miettinen, R., & Seppala, J. (1993). Effects of compatibilization on fractionated crystallization of PA6/PP blends. *Journal of Applied Polymer Science, 49*(7), 1165-1174.

Imholt, T. J., Dyke, C. A., Hasslacher, B., Perez, J. M., Price, D. W., Roberts, J. A., et al. (2003). Nanotubes in Microwave Fields: Light Emission, Intense Heat, Outgassing, and Reconstruction. *Chemistry of Materials, 15*(21), 3969-3970.

Ishai, O., & Cohen, L. J. (1967). Elastic properties of filled and porous epoxy composites. *International Journal of Mechanical Sciences, 9*(8), 539-546.

Iskander, M. (1993). Computer modeling and numerical simulation of microwave heating systems. *MRS Bulletin, 18*(11), 30-36.

Janney, M., & Kimrey, H. (1988). *Microstructure evolution in microwave sintered alumina*. Paper presented at the Annual Meeting of American Ceramic Society, Cincinnati, OH, USA.

Jarcho, M., Bolen, C., Thomas, M., Bobick, J., Kay, J., & Doremus, R. (1976).

Hydroxylapatite synthesis and characterization in dense polycrystalline form. *Journal of Materials Science, 11*(11), 2027-2035.

Kaya, C. (2008). Electrophoretic deposition of carbon nanotube-reinforced hydroxyapatite bioactive layers on Ti-6Al-4V alloys for biomedical applications. *Ceramics International, 34*(8), 1843-1847.

Kealley, C., Latella, B., van Riessen, A., Elcombe, M., & Ben-Nissan, B. (2008). Micro-and Nano-Indentation of a Hydroxyapatite-Carbon Nanotube Composite. *Journal of Nanoscience and Nanotechnology, 8*(8), 3936-3941.

Kearns, J., & Shambaugh, R. (2002). Polypropylene fibers reinforced with carbon nanotubes. *Journal of Applied Polymer Science, 86*(8), 2079-2084.

Kerner, E. H. (1956). The Elastic and Thermo-elastic Properties of Composite Media. *Proceedings of the Physical Society. Section B, 69*(8), 808.

Khor, K., Fu, L., Lim, V., & Cheang, P. (2000). The effects of ZrO2 on the phase compositions of plasma sprayed HA/YSZ composite coatings. *Materials Science and Engineering A, 276*(1-2), 160-166.

Kim, H., Chae, Y., Park, B., Yoon, J., Kang, M., & Jin, H. (2008). Thermal and electrical conductivity of poly (l-lactide)/multiwalled carbon nanotube nanocomposites. *Current Applied Physics, 8*(6), 803-806.

Kim, P., & Lee, D. (2009). Composite sandwich constructions for absorbing the electromagnetic waves. *Composite Structures, 87*(2), 161-167.

Kimura, T., Ago, H., Tobita, M., Ohshima, S., Kyotani, M., & Yumura, M. (2002). Polymer Composites of Carbon Nanotubes Aligned by a Magnetic Field. *Advanced Materials, 14*(19), 1380-1383.

Kissel, W., Han, J., & Meyer, J. (1999). Polypropylene: Structure, Properties,

Manufacturing Processes, and Applications. In H. Karian (Ed.), *Handbook of Polypropylene and Polypropylene Composites* (pp. 15-38): Marcel Dekker, Inc.

Kitagawa, K., Kanuma, Y., Oguro, T., & Harada, A. (1986). The reliability of magnetrons for microwave ovens. *Journal of Microwave Power and Electromagnetic Energy, 21*(3), 149-158.

Komarneni, S., Roy, R., & Li, Q. (1992). Microwave-hydrothermal synthesis of ceramic powders. *Materials Research Bulletin, 27*(12), 1393-1405.

Krieger, B. (1992). Vulcanization of rubber, a resounding success for microwave processing.. *Paper presented at the American Chemical Scociety Spring Meeting, San Franciso, CA, USA.* pp. 339-340.

Kurtz, S. M., Foulds, J. R., Jewett, C. W., Srivastav, S., & Edidin, A. A. (1997). Validation of a small punch testing technique to characterize the mechanical behaviour of ultra-high-molecular-weight polyethylene. *Biomaterials, 18*(24), 1659-1663.

Kurtz, S. M., Jewett, C. W., Bergström, J. S., Foulds, J. R., & Edidin, A. A. (2002). Miniature specimen shear punch test for UHMWPE used in total joint replacements. *Biomaterials, 23*(9), 1907-1919.

Kurtz, S. M., Jewett, C. W., Foulds, J. R., & Edidin, A. A. (1999). A miniature specimen mechanical testing technique scaled to articulating surface of polyethylene components for total joint arthroplasty. *Journal of Biomedical Materials Research, 48*(1), 75-81.

Lauf, R., Bible, D., Johnson, A., & Everleigh, C. (1993). 2 to 18 GHz broadband microwave heating systems. *Microwave Journal-Euroglobal Edition, 36*(11), 24-34.

Lee, G., Jagannathan, S., Chae, H., Minus, M., & Kumar, S. (2008). Carbon nanotube dispersion and exfoliation in polypropylene and structure and properties of the resulting composites. *Polymer, 49*(7), 1831-1840.

Li, S., Li, Z., Yang, M., Hu, Z., Xu, X., & Huang, R. (2004). Carbon nanotubes induced nonisothermal crystallization of ethylene-vinyl acetate copolymer. *Materials Letters, 58*(30), 3967-3970.

Liang, J. Z., Li, R. K. Y., & Tjong, S. C. (1998). Morphology and tensile properties of glass bead filled low density polyethylene composites: material properties. *Polymer Testing, 16*(6), 529-548.

Liao, S., Yen, C., Weng, C., Lin, Y., Ma, C., Yang, C., et al. (2008). Preparation and properties of carbon nanotube/polypropylene nanocomposite bipolar plates for polymer electrolyte membrane fuel cells. *Journal of Power Sources, 185*(2), 1225-1232.

Lidström, P., Tierney, J., Wathey, B., & Westman, J. (2001). Microwave assisted organic synthesis--a review. *Tetrahedron, 57*(45), 9225-9283.

Liu, X., & Wu, Q. (2001). PP/clay nanocomposites prepared by grafting-melt intercalation. *Polymer, 42*(25), 10013-10019.

Liu, Y., & Wang, M. (2007). Fabrication and characteristics of hydroxyapatite reinforced polypropylene as a bone analogue biomaterial. *Journal of Applied Polymer Science, 106*(4), 2780-2790.

Lo, J., Lu, Y., & Shinozaki, D. (2005). Kink band formation during micro-indentation of oriented polypropylene. *Materials Science and Engineering: A, 409*(1-2), 76-86.

Logakis, E., Pollatos, E., Pandis, C., Peoglos, V., Zuburtikudis, I., Delides, C. G., et al. (2010). Structure-property relationships in isotactic polypropylene/multi-walled

carbon nanotubes nanocomposites. *Composites Science and Technology, 70*(2), 328-335.

Lucas, G., Odette, G., Sokolov, M., Sp tig, P., Yamamoto, T., & Jung, P. (2002). Recent progress in small specimen test technology. *Journal of Nuclear Materials, 307-311*, 1600-1608.

Lynn, A., & DuQuesnay, D. (2002). Hydroxyapatite-coated Ti-6Al-4V: Part 1: the effect of coating thickness on mechanical fatigue behaviour. *Biomaterials, 23*(9), 1937-1946.

MacDonald, R., Voge, C., Kariolis, M., & Stegemann, J. (2008). Carbon nanotubes increase the electrical conductivity of fibroblast-seeded collagen hydrogels. *Acta Biomaterialia, 4*(6), 1583-1592.

Maier, C., & Calafut, T. (1998). *Polypropylene: the definitive user's guide and databook*: CRC.

Mao, X., Saito, M., & Takahashi, H. (1991). Small punch test to predict ductile fracture toughness JIC and brittle fracture toughness KIC. *Scripta Metallurgica et Materialia, 25*(11), 2481-2485.

Martuscelli, E., Silvestre, C., & Abate, G. (1982). Morphology, crystallization and melting behaviour of films of isotactic polypropylene blended with ethylene-propylene copolymers and polyisobutylene. *Polymer, 23*(2), 229-237.

McNally, T., Potschke, P., Halley, P., Murphy, M., Martin, D., Bell, S., et al. (2005). Polyethylene multiwalled carbon nanotube composites. *Polymer, 46*(19), 8222-8232.

Mendez, U., Kharissova, O., & Rodriguez, M. (2003). Synthesis and morphology of nanostructures via microwave heating. *Reviews on Advanced Materials Science,*

5(4), 398-402.

Meng, Y., Tang, C. Y., Tsui, C. P., & Chen, D. Z. (2008). Fabrication and characterization of needle-like nano-HA and HA/MWNT composites. *Journal of Materials Science: Materials in Medicine, 19*(1), 75-81.

Meredith, R. (1998). *Engineers' handbook of industrial microwave heating*: Inst of Engineering & Technology.

Metaxas, A., & Meredith, R. (1983). *Industrial microwave heating*: Inst of Engineering & Technology.

Mijuca, D. (2008). On a reliable finite element approach in multiscale multimaterial solid thermo-mechanics. *Journal of Serbian Society for Computational Mechanics, 2*(1), 44-62.

Misra, S., Valappil, S., Roy, I., & Boccaccini, A. (2006). Polyhydroxyalkanoate (PHA)/inorganic phase composites for tissue engineering applications. *Biomacromolecules, 7*(8), 2249-2258.

Moniruzzaman, M., & Winey, K. (2006). Polymer nanocomposites containing carbon nanotubes. *Macromolecules, 39*(16), 5194-5205.

Murugan, R., & Ramakrishna, S. (2005). Development of nanocomposites for bone grafting. *Composites Science and Technology, 65*(15-16), 2385-2406.

National Research Council (U.S.). Committee on Microwave Processing of Materials: An Emerging Industrial Technology, National Research Council (U.S.). National Materials Advisory Board, National Research Council (U.S.). Commission on Engineering and Technical Systems. (1994). *Microwave processing of materials*: National Academies Press.

Nielsen, L. E. (1970). Generalized equation for the elastic moduli of composite

materials. *Journal of Applied Physics, 41*, 4626.

Oghbaei, M., & Mirzaee, O. (2010). Microwave versus conventional sintering: A review of fundamentals, advantages and applications. *Journal of Alloys and Compounds, 494*(1-2), 175-189.

Olevsky, E. (1998). Theory of sintering: from discrete to continuum. *Materials Science and Engineering, 23*(2), 41-100.

Ozawa, T. (1971). Kinetics of non-isothermal crystallization. *Polymer, 12*(3), 150-158.

Palaith, D., & Silberglit, R. (1989). Microwave joining of ceramics. *American Ceramic Society Bulletin, 68*(9), 1601-1606.

Park, J., & Lakes, R. (1992). *Biomaterials: an introduction* (Second Edition ed.): Plenum Press.

Pasquini, N., & Addeo, A. (2005). *Polypropylene handbook*: Hanser Gardner Pubns.

Patterson, M. C. L., Apte, P. S., Kimber, R. M., Roy, R. (1992). *Batch Process for Microwave Sintering of Si_3N_4*. Paper presented at the Materials Research Society Proceedings, Microwave processing of materials III. Eds.: Beatty, R. L., Sutton, W. H., Iskander, M. F., Materials Research Society, Pittsburgh, *269*, 291-300.

Patterson, M. C. L., Kimber, R. M., Apte, P. S. (1990). *The Properties of Alumina Sintered in a 2.45 GHz Microwave Field*. Paper presented at Materials Research Society Proceedings, Microwave processing of materials II, Eds.: Synder, W. B., Sutton, W. H., Johnson, D. L., Iskander, M. F., Materials Research Society, Pittsburgh, *189*, 257-266.

Petit, P., Jouguelet, E., Fischer, J. E., Rinzler, A. G., & Smalley, R. E. (1997). Electron spin resonance and microwave resistivity of single-wall carbon nanotubes. *Physical Review B, 56*(15), 9275-9278.

Polizu, S., Maugey, M., Poulin, S., Poulin, P., & Yahia, L. (2006). Nanoscale surface of carbon nanotube fibers for medical applications: Structure and chemistry revealed by TOF-SIMS analysis. *Applied Surface Science, 252*(19), 6750-6753.

Pompe, W., Worch, H., Epple, M., Friess, W., Gelinsky, M., Greil, P., et al. (2003). Functionally graded materials for biomedical applications. *Materials Science and Engineering A, 362*(1-2), 40-60.

Porter, A., Taak, P., Hobbs, L., Coathup, M., Blunn, G., & Spector, M. (2004). Bone bonding to hydroxyapatite and titanium surfaces on femoral stems retrieved from human subjects at autopsy. *Biomaterials, 25*(21), 5199-5208.

Potente, H., Karger, O., & Fiegler, G. (2002). Laser and Microwave Welding - The Applicability of New Process Principles. *Macromolecular Materials and Engineering, 287*(11), 734-744.

Pujari, S., Ramanathan, T., Kasimatis, K., Masuda, J. i., Andrews, R., Torkelson, J. M., Brinson, C., Burghardt, W. R. (2009). Preparation and characterization of multiwalled carbon nanotube dispersions in polypropylene: Melt mixing versus solid-state shear pulverization. *Journal of Polymer Science Part B: Polymer Physics, 47*(14), 1426-1436.

Qian, D., Dickey, E., Andrews, R., & Rantell, T. (2000). Load transfer and deformation mechanisms in carbon nanotube-polystyrene composites. *Applied Physics Letters, 76*(20), 2868-2870.

Qiu, W., Mai, K., & Zeng, H. (2000). Effect of silane-grafted polypropylene on the mechanical properties and crystallization behaviour of talc/polypropylene composites. *Journal of Applied Polymer Science, 77*(13), 2974-2977.

Rahman, M., & Nor, S. (2009). An experimental investigation of metal powder

compaction at elevated temperature. *Mechanics of Materials, 41*(5), 553-560.

Rauwendaal, C. (2001). *Polymer extrusion*: Hanser Verlag.

Safadi, B., Andrews, R., & Grulke, E. (2002). Multiwalled carbon nanotube polymer composites: synthesis and characterization of thin films. *Journal of Applied Polymer Science, 84*(14), 2660-2669.

Saito, R., Dresselhaus, G., & Dresselhaus, M. (1998). *Physical properties of carbon nanotubes*: Imperial College Pr.

Savitskii, A. (2009). *Sintering of systems with interacting components*: Trans Tech Publications.

Savitskii, A., Tabachenko, A., Kwon, Y., Kim, J., Bae, J., & Moon, J. (2000). *Concentration dependence of volume changes during sintering of binary systems.* Paper presented at the Proceedings of The 4th Korea-Russia International Symposium on Science and Technology, University of Ulsan, S. Korea.

Seo, M. K., & Park, S. J. (2004). Electrical resistivity and rheological behaviours of carbon nanotubes-filled polypropylene composites. *Chemical Physics Letters, 395*(1-3), 44-48.

Shi, D. (2004). *Biomaterials and tissue engineering*: Springer Verlag.

Shi, D. (2006). *Introduction to biomaterials*: Tsinghua University Press.

Tadmor, Z., & Gogos, C. (2006). *Principles of polymer processing*: John Wiley and Sons.

Takahashi, T., Yonetake, K., Koyama, K., & Kikuchi, T. (2003). Polycarbonate crystallization by vapor-grown carbon fiber with and without magnetic field. *Macromolecular Rapid Communications, 24*(13), 763-767.

Tang, C. Y., Guo, Y., Tsui, C. P., & Gao, B. (2007). Multi-scale finite element analysis on biomechanical response of functionally graded dental implant/mandible system. *Journal of Serbian Society for Computational Mechanics, 1*(1), 164-173.

Tang, W., Santare, M. H., & Advani, S. G. (2003). Melt processing and mechanical property characterization of multi-walled carbon nanotube/high density polyethylene (MWNT/HDPE) composite films. *Carbon, 41*(14), 2779-2785.

Taniguchi, Y., Dohda, K., & Wang, Z. (2005). Effect of Lubrication on the Improvement of Uniformity in Uniaxial Powder Compaction. *JSME International Journal Series A, 48*(4), 393-398.

Tanner, K., Downes, R., & Bonfield, W. (1994). Clinical applications of hydroxyapatite reinforced materials. *British Ceramic Transactions, 93*(3), 104-107.

Thridandapani, R. R., Folgar, C. E., Kulp, A., Folz, D. C., & Clark, E. E. (2010). Effect of direct microwave sintering on structure and properties of 8 mol% Y2O3-ZrO2. *International Journal of Applied Ceramic Technology,* doi: 10.1111/j.1744-7402.2010.02570.x.

Thomas, S., & Yang, W. (2009). *Advances in polymer processing: macro-to-nano-scales*: Taylor and Francis.

Thostenson, E., & Chou, T. (1999). Microwave processing: fundamentals and applications. *Composites Part A: Applied Science and Manufacturing, 30*(9), 1055-1071.

Thostenson, E., & Chou, T. (2002). Aligned multi-walled carbon nanotube-reinforced composites: processing and mechanical characterization. *Journal of Physics D: Applied Physics, 35*(16), L77-L80.

Valentini, L., Biagiotti, J., Kenny, J. M., & Santucci, S. (2003). Effects of single-walled

carbon nanotubes on the crystallization behaviour of polypropylene. *Journal of Applied Polymer Science, 87*(4), 708-713.

Van Krevelen, D. W., & Te Nijenhuis, K. (2009). *Properties of polymers: their correlation with chemical structure; their numerical estimation and prediction from additive group contributions*: Elsevier Science Ltd.

Velasco, J., De Saja, J., & Martinez, A. (1996). Crystallization behaviour of polypropylene filled with surface-modified talc. *Journal of Applied Polymer Science, 61*(1), 125-132.

Vrijland, W. W., Jeekel, J., Steyerberg, E. W., Hoed, P. T. d., & Bonjer, H. J. (2000). Intraperitoneal polypropylene mesh repair of incisional hernia is not associated with enterocutaneous fistula. *British Journal of Surgery, 87*(3), 348-352.

Wadhawan, A., Garrett, D., & Perez, J. M. (2003). Nanoparticle-assisted microwave absorption by single-wall carbon nanotubes. *Applied Physics Letters, 83*(13), 2683-2685.

Wang, C. Y., Chen, T. H., Chang, S. C., Cheng, S. Y., & Chin, T. S. (2007). Strong Carbon-Nanotube-Polymer Bonding by Microwave Irradiation. *Advanced Functional Materials, 17*(12), 1979-1983.

Wang, H., Feng, J., Hu, X., & Ng, K. (2009). The formation of hollow poly (methyl methacrylate)/multiwalled carbon nanotube nanocomposite cylinders by microwave irradiation. *Nanotechnology, 20*(9), 095601.

Wang, M., Joseph, R., & Bonfield, W. (1997). *Influence of hydroxyapatite particle size and morphology on HAPEX(tm).* Paper presented at the Proceeding of the 10th International Symposium on Ceramic in Medicine, Paris, France.

Wang, M., Ladizesky, N., Tanner, K., Ward, I., & Bonfield, W. (2000). Hydrostatically

extruded HAPEX(tm). *Journal of Materials Science, 35*(4), 1023-1030.

Wang, M., & Pan, N. (2008). Predictions of effective physical properties of complex multiphase materials. *Materials Science and Engineering: R: Reports, 63*(1), 1-30.

Wang, S., Shen, L., & Tong, Y. (2005). Preparation and mechanical properties of chitosan/carbon nanotubes composites. *Biomacromolecules, 6*(6), 3067-3072.

Wang, Y., Fu, Q., Li, Q., Zhang, G., Shen, K., Wang, Y. (2002). Ductile–brittle-transition phenomenon in polypropylene/ethylene-propylene-diene rubber blends obtained by dynamic packing injection molding: A new understanding of the rubber-toughening mechanism. *Polymer Physics, 40*(18), 2086-2097.

Watts, P. C. P., Ponnampalam, D. R., Hsu, W. K., Barnes, A., & Chambers, B. (2003). The complex permittivity of multi-walled carbon nanotube-polystyrene composite films in X-band. *Chemical Physics Letters, 378*(5-6), 609-614.

White, A., Best, S., & Kinloch, I. (2007). Hydroxyapatite-carbon nanotube composites for biomedical applications: a review. *International Journal of Applied Ceramic Technology, 4*(1), 1-13.

Wiemann, K., Kaminsky, W., Gojny, F., & Schulte, K. (2005). Synthesis and properties of syndiotactic poly (propylene)/carbon nanofiber and nanotube composites prepared by in situ polymerization with metallocene/MAO catalysts. *Macromolecular Chemistry and Physics, 206*(15), 1472-1478.

Wiesbrock, F., Hoogenboom, R., & Schubert, U. S. (2004). Microwave-Assisted Polymer Synthesis: State-of-the-Art and Future Perspectives. *Macromolecular Rapid Communications, 25*(20), 1739-1764.

With, G., Dijk, H., Hattu, N., & Prijs, K. (1981). Preparation, microstructure and

mechanical properties of dense polycrystalline hydroxy apatite. *Journal of Materials Science, 16*(6), 1592-1598.

Wong, C. P., & Bollampally, R. S. (1999). Thermal conductivity, elastic modulus, and coefficient of thermal expansion of polymer composites filled with ceramic particles for electronic packaging. *Journal of Applied Polymer Science, 74*(14), 3396-3403

Wong, E. W., Sheehan, P. E., & Lieber, C. M. (1997). Nanobeam Mechanics: Elasticity, Strength, and Toughness of Nanorods and Nanotubes. *Science, 277*(5334), 1971-1975.

Wu, C., Chen, M., & Karger-Kocsis, J. (1998). Transcrystallization in syndiotactic polypropylene induced by high-modulus carbon fibers. *Polymer Bulletin, 41*(2), 239-245.

Wu, D., Sun, Y., Wu, L., & Zhang, M. (2008a). Linear viscoelastic properties and crystallization behaviour of multi-walled carbon nanotube/polypropylene composites. *Journal of Applied Polymer Science, 108*(3), 1506-1513.

Wu, D., Wu, L., Zhang, M., & Zhao, Y. (2008b). Viscoelasticity and thermal stability of polylactide composites with various functionalized carbon nanotubes. *Polymer Degradation and Stability, 93*(8), 1577-1584.

Wu, J., & Kong, L. (2004). High microwave permittivity of multiwalled carbon nanotube composites. *Applied Physics Letters, 84*(24), 4956-4958.

Xie, S., Li, W., Pan, Z., Chang, B., & Sun, L. (2000). Mechanical and physical properties on carbon nanotube. *Journal of Physics and Chemistry of Solids, 61*(7), 1153-1158.

Xu, D., & Wang, Z. (2008). Role of multi-wall carbon nanotube network in composites

to crystallization of isotactic polypropylene matrix. *Polymer, 49*(1), 330-338.

Yang, B., Pramoda, K., Xu, G., & Goh, S. (2007). Mechanical reinforcement of polyethylene using polyethylene-grafted multiwalled carbon nanotubes. *Advanced Functional Materials, 17*(13), 2062-2069.

Yu, M. F., Lourie, O., Dyer, M. J., Moloni, K., Kelly, T. F., & Ruoff, R. S. (2000). Strength and Breaking Mechanism of Multiwalled Carbon Nanotubes Under Tensile Load. *Science, 287*(5453), 637-640.

Zeng, H., & Lacefield, W. (2000). XPS, EDX and FTIR analysis of pulsed laser deposited calcium phosphate bioceramic coatings: the effects of various process parameters. *Biomaterials, 21*(1), 23-30.

Zhang, D., Kandadai, M., Cech, J., Roth, S., & Curran, S. (2006). Poly (L-lactide)(PLLA)/multiwalled carbon nanotube (MWCNT) composite: characterization and biocompatibility evaluation. *The Journal of Physical Chemistry B, 110*(26), 12910-12915.

Zhang, Y., & Tanner, K. (2003). Impact behaviour of hydroxyapatite reinforced polyethylene composites. *Journal of Materials Science: Materials in Medicine, 14*(1), 63-68.

Zhao, L., & Gao, L. (2004). Novel in situ synthesis of MWNTs-hydroxyapatite composites. *Carbon, 42*(2), 423-426.